united nations
educational, scientific
and cultural
organization

international atomic
energy agency

the
abdus salam
international centre for theoretical physics

SMR.1148 - 48

COLLEGE ON MEDICAL PHYSICS
AND
WORKSHOP ON
NUCLEAR DATA FOR SCIENCE AND TECHNOLOGY:
MEDICAL APPLICATIONS
(20 SEPTEMBER - 15 OCTOBER 1999)

"Medical Applications of the MCNP Monte Carlo Code"

Timothy D. SOLBERG
University of California @ Los Angeles
Department of Radiation Oncology
200 UCLA Medical Plaza
Suite B265
90095-6951 Los Angeles
U.S.A.

A Review of Radiation Dosimetry Applications using the MCNP Monte Carlo Code

Presented to the IAEA Workshop on Nuclear Data for Science and Technology:
Medical Applications, ICTP Trieste, Italy, October, 1999

Timothy D. Solberg, John J DeMarco, Indrin J. Chetty, Albert V. Mesa, Christopher H. Cagnon, Alex N. Li, Kali K. Mather, Paul M. Medin, Alonso R. Arellano, James B. Smathers

Department of Radiation Oncology, UCLA School of Medicine,
Los Angeles, California, USA

Correspondence to: Timothy D. Solberg, Ph.D.
Co-Director, UCLA Radiosurgery Program
Department of Radiation Oncology
200 UCLA Medical Plaza, suite B265
Los Angeles, CA 90095-6951
Solberg@radonc.ucla.edu

TABLE OF CONTENTS

ABSTRACT

The Monte Carlo code MCNP (Monte Carlo N-Particle) has a significant history dating to the early years of the Manhattan Project. More recently, MCNP has been used successfully to solve many problems in the field of medical physics. In radiotherapy applications MCNP has been used successfully to calculate the bremsstrahlung spectra from medical linear accelerators, for modeling the dose distributions around high dose rate brachytherapy sources, and for evaluating the dosimetric properties of new radioactive sources used in intravascular irradiation for prevention of restenosis following angioplasty. MCNP has also been used for radioimmunotherapy and boron neutron capture therapy applications. It has been used to predict fast neutron activation of shielding and biological materials. One area that holds tremendous clinical promise is that of radiotherapy treatment planning. In diagnostic applications, MCNP has been used to model X-ray computed tomography and positron emission tomography scanners, to compute the dose delivered from CT procedures, and to determine detector characteristics of nuclear medicine devices. MCNP has been used to determine particle fluxes around radiotherapy treatment devices and to perform shielding calculations in radiotherapy treatment rooms. This manuscript is intended to provide to the reader a comprehensive summary of medical physics applications of the MCNP code.

INTRODUCTION

The application of the technique to radiation transport problems is almost universally attributed to the work of Fermi in the late 1930s. Motivated by the development of the atomic bomb during the second world war, and encouraged by the advent of computers, Fermi, in collaboration with Ulam, von Neumann, Metropolis, and others, successfully demonstrated use of the technique to track neutral particles through a variety of materials [Br93]. Because charged particle interactions with matter are much more numerous and complex, some time passed before the seminal work on charged particle transport by Berger [Be63]. Based on this work, Berger and Seltzer developed ETRAN, the first general purpose computer code for photon and electron transport [Be68].

Even before the development of ETRAN, it was recognized that Berger's work may offer solutions to many of the problems encountered in dosimetry of ionizing radiation. In their 1967 text on radiation dosimetry, Fitzgerald, Brownell, and Mahoney state: "It seems that Monte Carlo techniques may well be the general method of choice in problems possessing complicated source and medium geometries" [Fi67]. The observation that the

applications be limited to "when deep penetrations are not of primary interest" shows that the authors appreciated the difficulties involved, including the computationally intensive nature of the method. While the years since the development of ETRAN have seen tremendous progress in the fields of radiation transport, radiation dosimetry, and algorithms for dose computation, the power of the Monte Carlo method remain unsurpassed. Most recently, Mohan has suggested "... there is a potential for an improvement in clinical outcome if accuracy in dose is improved with the aid of Monte Carlo simulation of radiation transport" [Mo97].

A number of investigators have adopted the MCNP (Monte Carlo N-Particle) Monte Carlo code as the framework on which to base dosimetry and radiotherapy treatment planning applications [Br93, Br97, He91]. The photon/electron transport in MCNP is based loosely on that of the Integrated Tiger Series (ITS version 1.0), which in turn has been adapted from ETRAN [Be68]. Though the Goudsmit-Saunderson formalism for multiple electron scattering in ETRAN/ITS is considered superior to other approaches, some deficiencies, particularly with regard to energy-loss straggling, have been noted [Ro86]. In the original implementation, energy-loss straggling is inadequately sampled from the Blunck-Leisegang approximation to the Landau theory. This deficiency was addressed in later versions of ITS [Se88] and recently implemented in MCNP [Br97, Hu97].

MCNP has a number of advantages that make it attractive for medical physics applications. The range for photon and electron transport extends from 1 keV to 100 MeV. Important low energy phenomena, such as the production and transport of characteristic x-rays and Auger cascades, are accurately modeled. The code also transports neutrons, though coupling extends only to neutron-produced photons; photoneutron production has only recently been implemented in MCNP though it is not presently supported in official releases. MCNP supports several geometry schemes simultaneously; the combinatorial geometry which combines first and second degree surfaces and fourth degree elliptical tori is ideally suited to accelerator modeling, while the nested lattice feature mimics voxel-based medical imagery. Multiple external radiotherapy beams can be easily simulated using the repeated structures feature. All directives from the user, including source configuration, target geometry, material specification, physics parameters, and biasing options, originate from a single text file; there is no user initiated written or compiled computer code. Yet modifications to the code are easily performed through the aid of the PRPR pre-processor. The ability to distribute a calculation over multiple, loosely connected computer processors allows the performance of MCNP to scale linearly with the number of processors dedicated to the task. MCNP is supported on numerous computer architectures and operating systems including Unix and Windows™ (DOS). Finally, three-dimensional visualization of MCNP geometry and particle

tracks is available though a separate application, SABRINA [We86]. The present MCNP code, version 4B, is in many ways a culmination of the work Fermi, Ulam, von Neumann, Metropolis, Berger and Seltzer. MCNP is actively supported by the XCI group at Los Alamos National Laboratory (www-xdiv.lanl.gov/XCI/PROJECTS/MCNP/).

This manuscript is intended as a general overview on the use of the MCNP code in medical dosimetry applications. For more specific details the reader is referred to the references herein. In addition, an excellent monograph on Monte Carlo applications in medical dosimetry is given by Andreo [An91]

EXTERNAL BEAM RADIOTHERAPY

Accelerator Modeling and Bremsstrahlung Production

Accurate calculation of bremsstrahlung spectra is a prerequisite to many other Monte Carlo calculations in medical radiation dosimetry. DeMarco et al used MCNP to calculate thick target bremsstrahlung spectra for 15 MeV electrons incident on targets of Al, Be, and Pb [De95]. At that time MCNP (version 4A) incorporated ITS version 1.0 electron transport [Ha84]. The default number of electron substeps was increased six-fold in each target material in order to minimize the surface artifact that results in an unrealistically high yield of bremsstrahlung photons produces in the forward direction. Integrated yield and mean energy of each spectrum was scored at various angles between 0 and 90 degrees. Results were compared with the measured data of Faddegon et al and with earlier calculations performed using the EGS4 code [Fa90, Fa91] and are summarized in Table 1. At angles less than 60 degrees, the integrated yield calculated using MCNP was within 6% of measured data for all target materials though at greater angles and for the Pb target in particular, MCNP overestimated measurement as well as EGS4 calculations. This is likely due to the outdated bremsstrahlung cross-section data in version 4A of MCNP. Calculations using new cross section data or improved electron transport of version 4B have yet to be performed.

To perform bremsstrahlung calculations for medical linear accelerators, detailed specifications of the accelerator's components are required from the manufacturer. In addition, the manufacturer must provide the energy distribution of the electrons on target though most often only the nominal energy is given. The accelerator is subsequently modeled in the Monte Carlo code and the resulting bremsstrahlung photons are produced and tracked through the various components (Figure 1). Next event estimators ("detectors" in MCNP) are widely used to score the resulting spectrum due to the inherent efficiency associated with their

use. A second series of calculations is performed to benchmark the quality of the spectra against measurement. Generally this consists of central axis depth dose and off-axis profiles in water. Due to inconsistencies in the specifications provided by the manufacturer, it is not uncommon to find some disagreement between the initial calculated depth dose and measurement. Thus this two-step process for obtaining and validating the photon spectra is an iterative one in that the electron energy on target is varied in the Monte Carlo simulation until agreement with measured data is reached.

Target	Angle	MCNP	EGS4	Experiment
Be	0	2.74×10^{0}	2.60×10^{0}	2.73×10^{0}
Be	2	2.10×10^{0}	2.00×10^{0}	2.14×10^{0}
Be	10	6.19×10^{-1}	5.69×10^{-1}	6.30×10^{-1}
Be	30	9.52×10^{-2}	8.65×10^{-2}	9.49×10^{-2}
Be	90	1.07×10^{-2}	9.89×10^{-3}	1.06×10^{-2}
Al	0	3.36×10^{0}	3.27×10^{0}	3.42×10^{0}
Al	2	2.68×10^{0}	2.63×10^{0}	2.78×10^{0}
Al	10	1.06×10^{0}	1.00×10^{0}	1.06×10^{0}
Al	30	2.71×10^{-1}	2.47×10^{-1}	2.65×10^{-1}
Al	90	3.38×10^{-2}	2.51×10^{-2}	2.87×10^{-2}
Pb	0	2.91×10^{0}	3.07×10^{0}	2.92×10^{0}
Pb	2	2.40×10^{0}	2.50×10^{0}	2.48×10^{0}
Pb	10	1.14×10^{0}	1.21×10^{0}	1.20×10^{0}
Pb	30	4.35×10^{-1}	4.50×10^{-1}	4.47×10^{-1}
Pb	90	5.94×10^{-2}	5.33×10^{-2}	5.19×10^{-2}

Table 1. Integrated bremsstrahlung yield (in Sr^{-1}) calculated using MCNP4A and EGS4 and measured by Faddegon et al [Fa91]. From DeMarco et al [De95].

Several investigators have performed calculations of bremsstrahlung spectra from medical accelerators using MCNP. Figure 2 shows spectra for 6 and 25 MV radiotherapy x-ray beams calculated by DeMarco et al [De98]. Though the nominal electron energy specified by the manufacturer is 6 and 25 MeV for the low and high energy modes respectively, the simulations required energies of 6.8 and 22.0 MeV in order to obtain good agreement with measurement. These spectra have undergone extensive benchmarking and are now used in Monte Carlo radiotherapy treatment planning applications (below) [De98, Ch99a].

In a similar fashion, Arellano et al and Chetty et al obtained spectra for a unique linear accelerator (Novalis) dedicated to radiosurgery applications (Figure 3) [Ar96, Ch99b]. This device has a considerably smaller flattening filter designed to increase radiation output. As a result, the beam is softer than that from other 6 MV accelerators, with an average energy of 1.67 MeV along the central axis and 1.40 MeV off axis.

Photon Beams

Monte Carlo applications in external beam radiotherapy have historically involved the calculation of standard beam parameters such as central axis depth dose and off-axis profiles. In addition, Monte Carlo is frequently used to obtain data where measurement is either not possible or there is significant uncertainty in the measured data. Solberg et al demonstrated that MCNP could be a valuable tool in predicting the dose near interfaces and in regions lacking in electronic equilibrium [So95]. Figure 4 demonstrates the loss of central axis equilibrium that can occur when photon beams encounter low density regions. Love et al compared calculated depth dose in water from several Monte Carlo codes including EGS4 and the two most recent versions of MCNP, the latter (MCNP4B) using two different energy indexing algorithms [Lo98]. Monoenergetic x-ray sources of 1.25, 1.9, and 3.0 MeV were used to approximate radiotherapy beams of Co-60 and 6 and 10 MV bremsstrahlung spectra respectively. Dose was scored as a function of depth in a simulated water phantom, then converted to dose per history to facilitate comparison between the codes. Beyond the depth of maximum dose, agreement between the three codes at all energies simulated was within the statistical uncertainty of the Monte Carlo calculations (< 2%). Within the buildup region, use of the default MCNP energy indexing algorithm resulted in a slightly lower calculated dose than either EGS4 or MCNP with improved energy indexing. The authors also noted that for the simple geometries used in their simulations, EGS4 was between 50 and 80 percent faster than MCNP.

The application of Monte Carlo techniques to radiotherapy treatment planning has been the subject of much recent speculation and discussion. Several academic centers, including UCLA, Stanford University, the Medical College of Virginia (MCV), Lawrence Livermore National Laboratory (LLNL), Memorial Sloan Kettering Cancer Center, and the National Research Council of Canada (NRCC) and others, are taking leading roles in the development of Monte Carlo treatment planning capabilities, though wide spread commercialization remains several years away [De98a, Ha96, Lo95, Ma98, Mo97, Ro90, Ro95, Wa97, Wa98c].

Use of MCNP for CT-based radiotherapy planning has been described by DeMarco et al, Wallace and Allen, and more recently by Chetty et al [Ch99a, Ch99b, De98a, Wa98c]. Wallace and Allen wrote custom FORTRAN code to construct voxels using on the standard MCNP combinatorial geometry. This is similar to the technique used by Zamenhof et al in boron neutron capture therapy applications (see below) [Za96]. Elemental composition and density were determined based on CT number according to ICRU Report 46. Further preprocessing was performed to separate the surrounding air from voxels of similar density within the lung. Transport was performed using an earlier version of MCNP (version 3A). Because version 3A does not transport electrons, the photon fluence was scored in each voxel and convolved with an appropriate KERMA factor. Approximately 10 hours of run time was required to obtain a standard deviation of 5% or less in each voxel. Other investigators have noted that smaller standard deviations may be necessary to produce "smoother" distributions.

DeMarco et al utilized the existing "lattice" geometry of MCNP, used traditionally for modeling of nuclear reactor elements, to facilitate use of voxel-based medical imagery. A graphical preprocessor was written to provide an interface the user and MCNP. The interface reads CT data and generates the MCNP lattice elements on grids of 64^2 to 512^2 matrices filled with one of 17 material/density designations based on CT number, following ICRP Report 23 and ICRU Report 44. The user specifies treatment specific parameters such as beam energy (bremsstrahlung spectra from a pre-calculated library of medical linear accelerators), orientation and the number of beams. All information is written to an MCNP input file that depending on the resolution desired for the dose (lattice) voxels, may be tens of thousands of lines long. Coupled photon/electron transport was performed using MCNP4A (with a fix for the energy straggling artifact pointed out by Rogers et al [Ro86]). Dose was scored in each lattice element using the energy deposition tally (*f8) modified for a heterogeneous lattice. Preprocessing functions, as well as post-processing functions for dose display and plan evaluation have since been integrated into a commercial treatment planning system.

Numerous benchmarks were performed to validate the approach in homogeneous and heterogeneous geometries. Figure 4 shows a comparison between MCNP and measurement for a solid water phantom with a low density region inserted. MCNP accurately predicts the loss of central axis equilibrium and the resulting secondary buildup region following the inhomogeneity. Conventional dose algorithms (EqTAR – also shown) fail to predict the perturbation by the low density region. Figure 5 shows a 4 field arrangement for irradiation of the prostate calculated using MCNP. The 60% isodose line in observed to follow the contour of the rectum. This is not the case when the identical plan is performed using a commercial

system. This has significant clinical implications as the rectum is the main dose limiting structure in irradiation of the prostate.

DeMarco et al have also made significant modifications to the MCNP code to optimize photon transport through the lattice geometry [De98a]. Furthermore, the user is allowed to specify only those particular voxels in which dose is to be scored. In radiotherapy applications where high dose resolution is desired and the voxels may be on the order of 1 mm, the tracking and scoring modifications have resulted in speedup of as much as 10^3.

Building on the work of DeMarco et al, Chetty et al have developed a generalized phase-space source for simulating among other things, field shaping using multileaf collimators and arbitrary intensity maps such as those used in intensity modulated radiotherapy (IMRT) [Ch99a, Ch99b]. Scoring of the x-ray is performed in a manner analogous to that described above. However, relative fluence values are interpolated from the phase space ring detectors to a cartesian grid using a simple polar coordinate transformation. Relative fluence for regions between ring detectors is obtained through linear interpolation (see Figure 6). Each source particle starting from the reconstructed phase-space source is assigned a position (x, y, z) by sampling a respective cumulative distribution function (CDF) for the virtual fluence grid. Figure 6 shows the primary fluence grid for a nominal 6 MV photon beam. A second CDF constructed in a similar manner is used to sample for the particle's energy. The source particle's direction is sampled by assuming that all particles originate from the target. Once the necessary CDFs are obtained, one can shape the phase space source to match the description of the physical beam by assigning appropriate relative fluence values to the corresponding grid elements. For example, in fields defined by a multileaf collimator, a value of 1.0 can be used to specify the open field while a value of 0.01 (determined through measurement) can be used to account for leakage through the collimators (Figure 7). Further enhancements have been made by the authors to account for the extrafocal source component and for scattering effects from tertiary collimation.

DeMarco et al and Chetty et al also made enhancements to the MCNP code to further improve performance [De98b, Ch99b]. First, the authors implemented the cut-point method for sampling from a CDF [Ch74]. This has resulted in a four-fold reduction of run times. Second, the authors implemented a delta scattering scheme (also known as Woodcock scattering) for photon transport in MCNP [Wo65]. In delta-ray scattering, the interaction cross section is broken into real and imaginary cross sections. For a collision scored as imaginary, the energy and direction of the particle are unchanged. The speedup for delta scattering is highly dependent on voxel size, from over 100 for voxels 0.5 mm on a side to approximately 20 for 1 cm voxels.

Figure 8 shows an example of a Monte Carlo treatment plan generated using the enhanced MCNP of Chetty and DeMarco, subsequently interfaced to a commercial planning system. The plan simulates a pseudo-stereotactic configuration of 17 beams, each of which has been shaped to the beams-eye-view projection of the tumor. The clinical implications of Monte Carlo treatment planning are evident in the dose-volume histogram. The Monte Carlo algorithm predicts a lower target dose (and lower spinal cord dose) than a commercial pencil beam algorithm.

Stereotactic Radiosurgery

Solberg et al performed an extensive series of benchmarks of the MCNP4A code for small photon beams (5-40 mm in diameter) such as those used in stereotactic radiosurgery. Small photon beams present particular difficulties for measurement due to finite sized detectors as well as lack of electronic equilibrium (side-scatter) along the central axis. Figure 9 shows a depth dose comparison between MCNP and measurement for a 6 MV photon beam mm in diameter. Agreement is excellent even within the buildup region. Small high energy beams such as these can undergo significant perturbation when tissue heterogeneities are encountered. The resulting distribution of dose is greatly influences by (lateral) electron transport and therefore cannot be predicted by conventional means. For example, small air cavities is an otherwise homogeneous medium will have the effect of reducing the dose beyond the distal interface. Figure 10 shows the dramatic effect that a 3 mm air cavity can have small photon beams. In the case of a 5 mm photon beam (often used for functional radiosurgery), dose is decreased at the distal interface by over one-third compared with the homogeneous case.

Subsequently, Solberg et al added a module for the simulation of CT-based radiosurgery treatment plans to the graphical user interface developed by DeMarco et al [De98a, So98]. Analogous to a clinical stereotactic radiosurgery (SRS) treatment planning system, the user provides isocenter position, Table angle, gantry start and stop angles, arc increment, and field (collimator) size. Like clinical systems, arcs are considered to be a series of fixed beams. Unlike clinical systems, however, the source spectrum is also easily varied. In this work several photon spectra, from Co-60 to 25 MV x-ray beams, differential in angle and energy, were obtained through prior MCNP calculations. Beams were modeled as simple point sources, with field size determined by sampling through an appropriate angle to provide the desired field size at isocenter. Differences between Monte Carlo and conventional algorithms are clearly evident in the single beam comparison shown in Figure 11. The conventional

algorithm fails to accurately predict the irregularities at the entrance surface as well the exit dose. The conventional algorithm also clearly fails to account for internal tissue heterogeneities. Figure 12 shows a similar comparison for multi-arc plans for a 30 mm diameter field passing through 460 total degrees. In this case the conventional algorithm overestimates the 90% dose volume by nearly 100 percent.

Recently Medin et al have proposed a system for accurate stereotactic radiosurgery of spinal targets [Me99]. The method relies on implantation of fiducial markers in the vertebral processes. As part of the initial project, the authors evaluated the dosimetry associated with small field irradiation of the vertebral column [Me96]. MCNP was used to evaluate the accuracy of conventional dose algorithms used in radiosurgery applications. Because radiosurgery is performed on intra-cranial targets, one underlying assumption in radiosurgery dose algorithms is that of tissue homogeneity. Figure 13 shows a treatment plan for a vertebral body target calculated using a conventional radiosurgery algorithm and one calculated using MCNP. The conventional algorithm overestimates each of the isodose volumes. In addition, the conventional algorithm underestimated the absolute dose at the center of the target by approximately 27%. Direct measurements confirmed both the relative and absolute dose predicted by MCNP.

Intensity Modulated Radiotherapy

Intensity modulated radiotherapy (IMRT) is a relatively new technique that seeks to improve on the limitations of conformal therapy through the use of non-uniform x-ray beams. The intensity profiles of the x-ray beams are determined through a computer-aided optimization process based primarily on the geometry of the patient's anatomy. In this process a large beam is subdivided into many small discrete elements. The intensity of each element is varied until an optimum dose distribution is achieved. Ultimately radiation is delivered in a series of field segments defined by a field-shaping device such as a multileaf collimator. These segments can in general be quite small and as pointed out by many investigators, conventional methods of dose calculations can break down in the absence of (lateral) electronic equilibrium. Thus there is a definite need for a technique such as Monte Carlo for IMRT dose calculations.

Monte Carlo simulations of IMRT are quite straightforward. Individual "pencil beam" elements can easily be simulated and the resulting dose distributions scored. However, the time involved in calculating each pencil beam element individually would be extremely prohibitive. By modeling the modulated beam using a source sampled off a phase-space gr

corresponding to the individual pencil beam elements (such as that developed by Chetty et al [Ch99]), this process can be made much more efficient.

X-Ray Phototherapy

X-ray phototherapy is a technique in which a tumor is loaded with a material of high atomic number (imaging contrast agents such as iodine and gadolinium are ideal compounds) and subsequently irradiated with kilovoltage x-rays. Large cross sections for photoelectric interactions in the contrast medium result in secondary radiations of auger cascades, characteristic x-rays, and photoelectrons, all high in linear energy transfer (LET). This contributes to a localized dose enhancement and hopefully superior tumor control. The technique was first proposed by Mello et al in 1983 [Me83]. Subsequently, experimental evidence has demonstrated dose enhancement in-vitro and in solid tumors [Iw87]. In 1990 Iwamoto et al modified a conventional CT scanner for x-ray phototherapy of brain tumors [Iw90]. The technique was subsequently evaluated in spontaneous canine brain tumors [No97]. More recently, the first experience of x-ray phototherapy to treat humans has been reported [No98, Ro99].

Primarily because photoelectric interactions are not accurately modeled by conventional techniques, Monte Carlo has been used extensively to support the dosimetry behind x-ray phototherapy. Initially Solberg et al used the MCNP code to confirm the depth dose characteristics of a CT-energy beam and to calculate dose enhancement factors: the ratio of dose to a target loaded with contrast material to that in a uniform (water) target [So92]. Figure 14 shows the good agreement in depth dose between MCNP and measurement. Mesa et al subsequently calculated dose enhancement factors for iodine and more recently several other potential dose enhancement agents [Me99]. In Figure 15 the dose enhancement factor (DEF) is plotted as a function of energy for three different iodine concentrations. The tradeoff between decreasing probability of a photoelectric interaction and increasing energy imparted to the photoelectron produces a DEF that peaks somewhat beyond the k-edge of iodine (33.2 keV) then decreases gradually to one.

Recently Mesa et al have used MCNP to investigate the dose distributions resulting from a multi-arc irradiation configuration such as that resulting from a modified CT scanner [Me99]. In this configuration the tumor is placed at the isocenter of the CT gantry. Radiation is delivered in three 360-degree rotations using gantry tilts of 0 and ± 20 degrees. Images from a cranial CT scan are used as input to the MCNP simulation following the method of DeMarco et al [De98a]. A region of interest 20 mm in diameter is constructed and the voxels

are artificially manipulated to have an appropriate material and density corresponding to up to 15 mg/ml of iodine. Figures 16-17 show the resulting dose distributions calculated by MCNP. With no iodine contrast material present the skull and intervening tissue receive substantial dose, in some locations nearly equal to that of the target. As the iodine concentration is increased to 15 mg/ml, the dose distributions become more tightly focused around the tumor and the peripheral dose to the bone is substantially reduced. In addition, though a conventional 10 MV stereotactic treatment does not suffer from the enhanced bone dose that occurs from treating with kilovoltage x-rays, the dose distributions from the low energy source rival do conform more tightly to the tumor (Figure 17). Finally, within the tilt limitations of the CT gantry three arcs appears to be the optimal number above which the bone dose again becomes limiting.

Electron Beams

There are numerous references in the literature describing the application of Monte Carlo techniques to electron beam dosimetry. In the case of MCNP however, little has been written. Love et al used EGS4 and MCNP-4B to calculate central axis depth dose in water for a 10 MeV electron beam [Lo98]. When MCNP is run in the default mode, the authors observed lower surface dose and deeper penetration compared with EGS4, a phenomenon due to incorrect energy indexing as pointed out earlier Jeraj et al [Je99]. When the improved energy indexing scheme is used, EGS4 and MCNP agree with each other within the statistical uncertainty of the calculations. Agreement at D50 (the distal depth of 50% dose) with BJR-25 calculations is within 0.5%.

Jeraj et al performed a similar study for 6 and 20 MeV electron beams [Je99]. The authors observed similar phenomena with regard to MCNP electron transport. At 6 MeV, both MCNP-4A and MCNP-4B using the default energy indexing ($MCNP_{DEF}$) underestimated energy loss, producing a beam that was too penetrating when compared to EGS4 and measurement. MCNP-4A incorrectly samples for energy straggling while $MCNP_{DEF}$ used the older method of energy indexing. The ETRAN formalism for energy straggling in MCNP-4A underestimates energy loss and has been described previously [Ro86]. However, with the improved MCNP energy indexing scheme (the authors refer to this as $MCNP_{ITS}$ for ITS-style indexing), MCNP calculations were in excellent agreement with measurement. For 20 MeV electrons, EGS4 and $MCNP_{ITS}$ were again in good agreement.

Jeraj et al also performed a series of calculations of electron backscatter near interfaces of air, copper, or lead and solid water [Je99]. Measurements were performed in a 20 MeV

electron beam using TLD and a parallel plate ionization chamber. EGS4 and MCNP-4B Monte Carlo simulations modeled the TLDs and used combined electron/photon spectrum. The electron backscatter factor (EBF) was defined as the ratio of dose to the TLD with and without the lead inhomogeneity. The authors note that the agreement between all versions of MCNP and measurements is good despite the fact that the depth dose is incorrectly calculated in earlier versions of MCNP. The authors also note that EGS4 calculations agreed well with measurement near air/water and copper/water interfaces, but EGS4 underestimated the EBF when lead was used. Results of their calculations and TLD experiments are summarized in Table 2.

With the added emphasis on electron transport in the recent versions of MCNP, the reader is referred to articles on the ITS series of codes. An excellent discussion on electron transport can be found in the proceedings edited by Jenkins, Nelson, and Rindi [Je88].

Pd position from entrance (mm)	TLD position from Pb (mm)	EBF (MCNP)	EBF (EGS4)	EBF (Measured)
54	0	1.41 ± 0.01	1.34 ± 0.01	1.43 ± 0.02
54	3	1.23 ± 0.01	1.20 ± 0.01	1.25 ± 0.02
34	3	1.22 ± 0.01	1.17 ± 0.01	1.20 ± 0.02
74	3	1.16 ± 0.01	1.18 ± 0.01	1.22 ± 0.02

Table 2. Electron backscatter factors near a lead/solid water interface calculated using EGS4 and MCNP and measured using TLD. From Jeraj et al [Je99].

Neutron Capture Therapy

MCNP has long been considered the code of choice for neutron and coupled neutron/photon transport. Thus it comes as no surprise that much of the dosimetry of neutron capture therapy (NCT) has been supported by MCNP. The aim of neutron capture therapy is to deliver a compound to a tumor which when radiated with neutrons will to produce short range/high LET reaction products. In boron neutron capture therapy (BNCT), the desired reaction, $^{10}B(n,\alpha)^{7}Li$, has a high capture cross section for thermal neutrons (> 3500 barns) and emits short ranged particles (< 10 μm in tissue) of high LET. Obviously the tumor specificity of the compound used is of great importance. However, the clinical issues of tumor specificity, toxicity, and patient results will not be discussed here.

One of the initial uses of MCNP in NCT was reported by Yanch et al 1991 [Ya91]. The authors used MCNP to determine the optimal neutron energy for treating brain tumors with

NCT. The brain and skull were modeled as ellipses and calculations carried out using mono-energetic neutron beams. Dose enhancement due to the boron component was obtained by multiplying the neutron flux by a factor of 3 or 30, corresponding to normal brain and tumor respectively, then applying the appropriate fluence-to-kerma factors. Several important conclusions that suggested future direction for clinical NCT were reached in the study. First, the optimal range of neutron energies for the treatment of brain tumors appears to be between 4 eV and 40 keV. The optimum field size also depends strongly on tumor size, shape and depth. Finally, calculations suggested that the largest depth well treated by NCT was approximately 10 cm and this was attainable with an energy of 10 keV.

Later, Yanch et al used MCNP in the design of a ^{252}Cf facility for BNCT [Ya93]. Various moderator/filter/reflector materials and configurations were investigated in an attempt to optimize the resulting clinical beam. Methods following their earlier work were used for simulation of the phantoms and for calculating the dose. Unfortunately the resulting dose rates were substantially lower than for reactor sources and the authors concluded that a clinical facility using even very large amounts of ^{252}Cf (1.0 g) was not feasible.

Gupta et al were one of the first groups to use MCNP to investigate the impact of the high energy (2.2 MeV) capture gamma rays that originate from the $^{1}H(n,\gamma)^{2}H$ interaction in BNCT [Gu93]. Depth dose and off axis profiles were generated by scoring the gamma flux using a track-length estimator (f4 tally) and applying the appropriate kerma factors. Results were compared with those using the QAD-CGGP code, a point kernel shielding code also developed at Los Alamos National Laboratory.

Pettersson et al used MCNP3B to calculate neutron and photon fluences at the Studsvik thermal neutron facility [Pe93]. A planar neutron source with a fission energy spectrum was modeled and fluences were tallied at the exit of the heavy water moderator and along the axis of the biological experiment tube. Calculations showed the neutron fluence to be reasonably homogeneous with the tube. Calculated thermal neutron rates radially and at depth along the tube agreed well with activation foil measurements. Photon dose within the tube was also calculated by multiplying the photon fluence by fluence-to-dose conversion factors. Calculated photon dose was in good agreement with that measured with TLD.

Konijnenberg et al have used MCNP to investigate neutron fluence distributions in water phantoms radiated by an epithermal neutron beam [Ko93]. Neutron fluence was divided into three energy bins: thermal (< 0.55 eV), epithermal (0.55 eV to 02 keV) and fast (> 20 keV). Foil activation as a function of depth was calculated and compared with measurement. At depths greater than 4 cm, calculated values were in excellent agreement with measurement. At depths less than 4 cm, however, measured data significantly overestimated the MCNP

calculations. The authors speculate this is a shortcoming in their measurement technique and not a problem with MCNP. The authors also investigated the effect of various beam modifying devices such as wedges and a borated polyethelyne/lead block. While the spatial distribution of thermal neutrons is relatively unaffected by the presence of wedges, the fast neutron spectrum is significantly altered.

In 1995, the same group performed a detailed analysis of BNCT dose distributions from multiple beam arrangements [Ko95]. Elliptical models of the head, skull and tumor were constructed to study the distribution of thermal neutrons and dose under realistic conditions. A 1 cm^3 cubic mesh in which tallies were made was superimposed over the head model. Assumptions were made as to the boron concentration in the skull, normal brain, and tumor in a 2:1:6 ratio. Simulations were performed in a two step approach. First, a detailed calculation of the reactor core, neutron port and filter was performed. This spectrum was used in subsequent simulations to score fluence and dose in the head model and to investigate the effect of beam modifying devices. This is analogous to the two-step process for the simulation of photon beam radiotherapy described above. Neutron dose was calculated using the appropriate kerma factors. The dose from capture gamma rays was included by assuming the presence of electronic equilibrium in the whole brain volume with the further assumption that the entire energy was deposited with the 1 cm^3 voxel. The authors also used the transformation feature (TR card) in MCNP to facilitate multi-port irradiation, demonstrating improved target dose homogeneity with multiple fields.

Wallace et al performed further Monte Carlo simulations of BNCT with the Petten high flux reactor epithermal neutron beam [Wa95]. As in earlier studies, the brain and skull were modeled as ellipses. However, the effect of heavy water as the constituent brain material in place of water was investigated. Gamma radiation from the source was not included in the simulation but neutron-induced photons were produced and tracked. Neutron and photon fluences were scored in 0.125 cm^3 tally volumes; fluence was converted to dose using the appropriate kerma factors. Deeper neutron penetration through the heavy water was observed compared with standard water, creating a higher thermal neutron component at the target depth. In addition, the gamma component was reduced due to fewer hydrogen capture reactions.

A patient-specific system for BNCT treatment planning has been described by Zamenhof et al [Za96]. Non-contrast computed tomography (CT) scans are used to generate an accurate three-dimensional model of the patient's anatomy suitable for use with MCNP. The images are automatically segmented into three tissue types: air, normal brain, and bone. Manual region of interest definition is used to segment the target; boron concentrations in the

target, normal tissue and blood are assigned manually based on a prior study. Individual $1cm^3$ cells are automatically generated using the standard MCNP combinatorial geometry; a typical MCNP simulation will consist of 11,205 of these cells.[1] Graphical tools allow the manipulation of various beam parameters including orientation and field size. Dose is computed using the appropriate kerma factors; electron transport was not included in the simulations. Post processing tools allow visualization of one dimensional profiles and two dimensional isodose distributions superimposed over the appropriate CT images. A specialized phantom was constructed for the purpose of verifying the treatment planning calculations. Excellent agreement was observed in the measured dose rates (thermal neutron, fast neutron, B-10, gamma and total) compared with the MCNP results.

One group has used Monte Carlo techniques to investigate possible dose enhancement in boron from fast neutron beams [Pi98, Pi99]. Neutron production, from 60 MeV cyclotron protons on a beryllium target, is modeled using the FLUKA code. The transport of the resulting primary neutrons is simulated using MCNP4A. The thermal spectrum was scored as a function of depth in a plexiglas phantom. Thermal neutron yield was observed to have a large field size dependence, with the yield at 20 x 20 cm^2 2.2 times that of 10 x 10 cm^2. Dose enhancement due to the thermal neutron capture by ^{10}Boron, assuming a concentration of 100 μg ^{10}B per gram of tissue, ranges from 4.6 to 10.4 percent of the fast neutron dose (Table 3).

Bleuel et al have also investigated accelerator neutron sources for BNCT, in this case a novel DC accelerator designed for a proton beam current of 100 mA [Bl98]. Neutrons are produced via a $^7Li(p,n)^7Be$ reaction. In a two-step process, the authors investigated the moderation effect of three materials: Al/AlF_3, ^7LiF, and heavy water. In the first step, MCNP was used to transport the neutron beam produced by the accelerator through the moderator assembly, scoring the neutron and gamma fluxes at the exit. In the second step, the BNCT-RTPE code, developed at the Idaho National Engineering and Environmental Laboratory [We97], was used to transport the epithermal neutrons and gammas through a model of a human head. A tumor concentration of 10 ppm ^{10}B was assumed. Analyzing the resulting dose distributions the authors found Al/AlF_3 and ^7LiF to be superior moderating materials, increasing the thermal neutron fluence and dose at the midline of the brain by as much as a factor of two over D_2O.

[1] More recently, the authors' use of cells created using the combinatorial geometry has been replaced by the MCNP lattice geometry.

	Dose Rate (Gy/s)		
Field Size (cm^2)	Fast Neutrons	$^{10}B(n,\alpha)^7Li$	Dose Enhancement (%)
10 x 10	2.368×10^{-3}	1.145×10^{-4}	4.6
20 x 20	2.672×10^{-3}	3.111×10^{-4}	10.4

Table 3. Dose rate from cyclotron-produced fast neutrons and that due to boron capture from the thermal component. From Pignol et al [Pi98].

Robert Brugger's group at the University of Missouri-Columbia has made a number of significant contributions in the areas of neutron therapy, neutron capture therapy, and Monte Carlo methods. In 1990, they were one of the first groups to use MCNP to study the optimization of neutron beam parameters for neutron capture therapy [Br90]. In 1992 they proposed the use of ^{157}Gd as a candidate for BNCT; MCNP was used to calculate the gamma dose from ^{158}Gd [Sh92]. This work was followed shortly by another investigation of the combined effects of interstitial ^{235}U sources combined with external beam neutron irradiation (see below) [Li92]. In 1994 the group reported on a design study of high intensity epithermal neutron facility at the Brookhaven Medical Research Reactor [Li94]. As in their previous work, MCNP was used to calculate the neutron and gamma fluxes and absorbed doses produced.

Fast Neutron and Heavy Ion Therapy

MCNP was originally designed as a neutron and fission code and is generally considered to be an excellent code for neutron transport. Because of this, citations in the literature using MCNP in neutron and coupled neutron/photon applications are numerous. In the specific area of medical dosimetry, however, there are few references regarding fast neutron transport.

Kleck et al have investigated tissue activation, in particular, the production of positron emitting isotopes, in patients undergoing fast neutron therapy [Kl91]. MCNP was utilized to calculate the production of ^{11}C, ^{13}N and ^{15}O in acrylic and water from the p(46)Be(20) cyclotron beam at the UCLA Neutron Therapy Facility. The neutron source was modeled as a planar disk 1 cm in diameter; the energy distribution was obtained from previously published data. Neutron collimators of the isocentric gantry were modeled to produce field sizes projecting 6 x 6 to 20 x 20 cm^2. ^{11}C, ^{13}N and ^{15}O production were calculated with the aid of specific reaction cross sections obtained from the literature. Similar activation calculations

were performed for high energy (20 – 50 MeV) photons produced from a racetrack microtron. Again, reaction specific cross sections were used within MCNP. Phantoms were subsequently irradiated and the activation characterized using autoradiography and positron emission tomography.

Bohm et al have reported the use of Monte Carlo techniques to model three fast neutron therapy facilities (at Fermi National Accelerator Laboratory, Harper Hospital in Detroit, Michigan, and the National Accelerator Centre in Faure, South Afirca) [Bo99]. The authors characterized each facility in a three step process. First, the LAHET code was used to transport incident particles on target to score the resulting neutron spectrum. MCNP was used to transport the resulting neutrons through the beam delivery system. Because LAHET and MCNP use the same combinatorial geometry scheme, this process was easily facilitated. Additional nuclear data libraries were added for use with MCNP. Finally, the PEREGRINE code was used to transport the neutrons through various phantoms and score the dose. In PEREGRINE, a two-source model of the incident neutron beam was used; primary neutrons, those that originate from the target and scattered neutrons, those that have interacted with the components along the beam path. A comparison of central axis depth dose and transverse prfiles showed excellent agreement between calculations and measurement.

BRACHYTHERAPY

Conventional Brachytherapy

Monte Carlo methods have found extensive use in the area of brachytherapy. One of the primary reasons for this is the difficulty involved in making direct measurements in the immediate proximity of a brachytherapy source. The concept of applying Monte Carlo techniques to brachytherapy originated in the early 1980s [Bu83, Da82, Wi83]. Since that time there has been extensive research in this area. One of the foremost proponents of the technique has been Williamson. Using a Monte Carlo code of his own design, and incorporating photon transport only, Williamson calculated some of the first dosimetric parameters for low energy sources and pointed out significant discrepancies with existing data [Wi88a, Wi88b]. Much of the original data calculated by Williamson has found its way into commercial treatment planning systems.

Use of MCNP for brachytherapy calculations is less common than for other codes, primarily EGS4 and that of Williamson. Within the last several years, however, MCNP citations in the literature have increased in number. MCNP has several nice features that make

it well suited to brachytherapy source modeling. The robust combinatorial geometry makes simulation of complex seed geometries very straightforward. Flux, kerma, or dose tallies can be performed in simple cylindrical or spherical geometries or in a regular lattice geometry. Low energy photon and electron transport in the most recent version of MCNP is also considered to be quite good.

In the early 1990s, Mason et al and MacPherson and Battista used MCNP to calculate dosimetric parameters of ^{169}Yb, a new low energy brachytherapy source [Ma92, Ma95]. The authors used MCNP-4A to model accurately the seeds to account for factors such as photon attenuation, self-absorption and scattering. Angular dose profiles at various distances as well as the dose rate constant Λ_0 were calculated and compared with TLD measurement. Calculated dose was determined by scoring the energy fluence (using a track length estimator) and multiplying by the mass-energy transfer coefficient. Calculated dose distributions agreed with measurement within approximately 5%. This is particularly good considering somewhat obsolete low energy photon cross section used by MCNP4A and recently pointed out by other investigators [De99]. Calculated source strength agreed with measurement within the statistical uncertainty of both techniques (Table 4).

Seed	Λ_0 (cGy h-1 U-1)	Technique
Type 8	1.34 ± 0.10	Measured
Type 8	1.25 ± 0.05	MCNP4A
Type 6	1.25 ± 0.05	MCNP4A

Table 4. Measured and calculated dose rate constant for a new ^{169}Yb brachytherapy source From MacPherson et al [Ma95].

Wuu et al used MCNP and a second code, DELTA, to estimate the relative biological effectiveness (RBE) of four brachytherapy sources relative to ^{60}Co [Wu96]. MCNP calculations were performed to generate the electron slowing down spectrum. From this the lineal energy spectra were determined and compared to measurements performed with a wall-less proportional counter constructed with no metals parts. Experimental and calculated results were in good agreement. Estimates of RBE were also in good agreement with published biological data (Table 5).

	Mean Lineal Energy			
Radionuclide	Monte Carlo	Measured	RBE	RBE
^{103}Pd	3.3	3.8	2.3	1.9 ±0.6[1]
^{125}I	3.0	3.5	2.1	1.4 ±0.6[1]
^{241}Am	3.1	3.5	2.1	
^{192}Ir	1.9	2.0	1.3	1.45[2]
^{60}Co	1.5	1.6	1.0	
[1]Ling et al [Li95], [2]Zellmer et al [Ze94]				

Table 5. Mean lineal energy and RBE calculated using MCNP for four brachytherapy sources. RBE values in the right hand column are from biological measurements. From Wuu et al [Wu96].

Several groups have used MCNP to investigate dosimetric properties of high dose rate ^{192}Ir sources [Fe96, Wa98b, Wa98d, Wa98e]. Fessenden et al used MCNP to calculate dosimetric parameters for a two ^{192}Ir HDR sources [Fe96]. Dose to a point in water was determined using two different MCNP kerma calculations (and assuming local deposition of electron energy); the kerma tally (f6) and a fluence tally (f5) modified by the appropriate energy absorption coefficients. ^{192}Ir point source calculations were performed and compared with prior studies. In addition, two commercial ^{192}Ir sources were modeled in their entirety. Measurements using GAF chromic film were performed to confirm calculations. Figure 18 shows the dose from one commercial ^{192}Ir source as a function of radial distance (with $1/r^2$ effects removed). Data agree well with the previous calculations of Williamson and Li [Wi95]. Other dosimetric parameters calculated with MCNP are also in good agreement with previously published data (Table 6).

	Air Kerma Strength (Sk)		
	192 Ir Point source	Vari-Source	Micro-selectron
Calculated (MCNP4A)	4.044	3.833	3.658
Reported Previously	4.110[1]		
[1]Glasgow and Dillman			

	Dose Rate Constant (Λ)		
	192 Ir Point source	Vari-Source	Micro-selectron
	1.111	1.043	1.111
	1.110[2]		1.115[2]
[2]Williamson and Li [Wi95]			

Table 6. Dosimetric parameters for a ^{192}Ir point source and two commercial HDR sources. From Fessenden et al [Fe96a].

Dosimetric characteristics of a commercial HDR ^{192}Ir source (Nucletron's MicroSelectron) were investigated by Wallace et al [Wa98b]. MCNP was used to provide an exact model of the source; 33 emissions were included in the modeled gamma ray spectrum. Toroidal tally volumes were used to scored dose (using the MCNP *f8 tally) radially outward from the source. An average value of 2.24 photons/decay was used to convert to units of per activity. Dose characteristics were in excellent agreement with the earlier calculations of Williamson and Li (who used a code of their own design) [Wi95]. The authors suggested that the departure from the inverse square law in the near field were due more to noted geometry than to buildup effects. The authors also suggested that a shift to CT-based brachytherapy treatment planning, increasingly common particularly in the case of permanent implants, should be accompanied by better dose algorithms than those presently employed in commercial systems.

Watanabe et al used MCNP to generate dosimetric data for a specialized HDR brachytherapy applicator [Wa98d, Wa88e]. The complex geometry of the applicator and its construction of stainless steel and tungsten present difficulties in both simulation and measurement. Photon fluence was scored using next-event generators (in MCNP the point and ring detector tally, f5). Rather than scoring dose directly as Wallace et al [Wa98b], dose was determined my multiplying calculated fluence by the appropriate mass absorption coefficients. The Monte Carlo simulation included 31 emissions in the modeled gamma ray spectrum. Conversion to units per activity was performed assuming an average value of 2.36 photons/decay. Here again some differences are noted between the present work and that of Wallace et al. The authors do note that there are four the principle energies that comprise the majority of emissions so any differences are expected to have an insignificant effect. Results compared favorably with those of previous studies [Na95, Wi91] and with direct measurements using TLDs. The authors suggest use of their 3D lookup tables based on Monte Carlo data to include applicator shielding and other effects that otherwise can produce significant errors.

In a manner similar to many earlier Monte Carlo studies, Wierzbicki et al have used MCNP to calculate reference dosimetric parameters of a new ^{125}I source [Wi98]. Radial dose function, anisotropy factors and anisotropy constants were determined by scoring the absorbed dose (using the MCNP *f8 tally) in a spherical water phantom. The seeds, consisting of four ^{125}I-impregnated resin beads encapsulated in Titanium tubes, were modeled in their geometric entirety. Small differences between calculated values and those measured by previous investigators were observed (Table 7). The authors speculate the differences are

primarily due to the phantom materials used in earlier measurements; they recommend use of the Monte Carlo values for clinical applications.

Anisotropy Factor				
Transverse Distance (cm)	Model 6711 Seed Measured[1]	Model 6702 Seed Measured[1]	IoGold Seed Measured[2]	IoGold Seed MCNP
0.5				0.975
0.75				0.955
1.0	0.944	0.968	0.885	0.946
1.5				0.951
2.0	0.936	0.928	0.847	0.945
3.0	0.893	0.897	0.926	0.947
4.0	0.887	0.942	0.853	0.951
5.0	0.884	0.959	0.936	0.952
Anisotropy Constant	0.93	0.95	0.90	0.95
[1]Nath et al [Na95]; [2]Wallace and Fan [Wa98a].				

Table 7. Monte Carlo calculations for the IoGold ^{125}I seed compared with measurement. From Wierzbicki et al [Wi98].

The accuracy of a commercial brachytherapy treatment planning system with regard to near field dosimetry, in particular, the superposition effect of multiple source locations, was investigated by Wong et al [Wo99]. They followed the methodology of their earlier work in determining dosimetric parameters for an ^{192}Ir source [Wa98b]. Results were compared with a commercial treatment planning system. The authors concluded that both the radial dose and anisotropy functions in the commercial system contained errors at distances less than 1 cm from the source. This in turn caused the commercial system to overestimate the dose to a point from multiple source (dwell) positions from 3 to 15 percent.

Most recently DeMarco et al have used MCNP to model two and three-dimensional dose distributions from permanent ^{125}I implants for carcinoma of the prostate [De99].

Intravascular Brachytherapy

Radiation of cardiac and peripheral arteries has recently been proposed as a mechanism for reducing restenosis following angioplasty procedures. Intravascular placement of radioactive sources may allow delivery of effective doses to the vessel wall while minimizing the peripheral dose to surrounding tissues. At this time several source designs are in use, each with several advantages and disadvantages. Two groups have used MCNP extensively to investigate dosimetric properties of intravascular sources [Fe96a, Fe96b, Li98].

Fessenden et al performed a detailed analysis of factors influencing the dose distribution from intravascular beta irradiation [Fe96b]. These factors included: beta source selection (^{32}P or ^{90}Sr/^{90}Y), source length, encapsulation, and effects of delivery catheter composition and thickness, location within the vessel, and vessel composition. ^{32}P and ^{90}Sr/^{90}Y beta sources were benchmarked against published data. Calculations were performed using MCNP version 4A with a patch incorporated to correct for the energy straggling artifacts pointed out by previous investigators [Ro86]. The patch, described by Hughes et al [Hu97] has since been incorporated into MCNP4B. Figure 19 shows dose as a function of distance for a ^{32}P point source calculated using MCNP. Monte Carlo calculations of several prior studies are shown for comparison. Agreement is generally good with differences apparent only within the first 1 mm. It should be noted that the calculations of Prestwich et al were performed with ETRAN which incorrectly samples the energy straggling distribution. Figure 20 shows similar comparisons for a ^{90}Y point source. Subsequently, a ^{90}Sr/^{90}Y source was designed and fabricated by the authors. A comparison of MCNP calculations to measurement demonstrated excellent agreement (Figure 21).

Li et al described the use of MCNP in obtaining dosimetric data for a novel radioactive stent (a stent is a mechanical device used to prevent arteries from collapsing following angiographic procedures) [Li98]. The source was constructed by bombarding a commercial stent with 8.5 MeV protons from the UCLA Neutron Therapy Facility cyclotron. The ^{48}Ti in the stent (45.2% composition) absorbs a proton forming ^{48}V. The resulting ^{48}V isotope decays by positron emission and electron capture with a half-life of 16 days. The primary decay emission are a 0.696 MeV max positron, 511 keV annihilation photons, and several other gamma rays in the range 0.944 to 2.241 MeV.

Due to the complex geometry of the stent, Monte Carlo simulations of individual elements (struts) were modeled using MCNP for reconstruction offline. The dose distribution of the entire stent was determined by combining that of an individual strut according to the stent geometry. Calculations were compared with subsequent measurements performed using

GAF chromic film in a specially constructed polystyrene phantom. A simple depth dose comparison is shown in Figure 23. Two-dimensional dose distributions taken at different levels on the stent are shown in Figure 24.

Other Brachytherapy Applications

Cf-252

DeMarco et al have used MCNP to calculate dose distributions from the source neutrons and photons as well as capture gammas from ^{252}Cf proposed as a brachytherapy source [De96]. Encapsulation of the ^{252}Cf source was modeled though the exact neutron cross-sections were not available for all materials. Source neutrons and capture gammas were considered in one simulation while source photons were accounted for in a separate simulation. The radial dose distribution was tallied using concentric cylinders. A kerma tally (f6) was used to score the dose distribution from source particles while dose from capture gamma was scored directly (*f8). Calculated data was compared against measurement and previous calculations. Neutron and photon dose rates of 2.02 and 1.25 cGy/hr/μg at a distance of 1 cm from the source were calculated from the proposed source.

U-235

A combination brachytherapy and neutron capture therapy technique using ^{235}U has been proposed by Liu et al [Li92]. The premise is that ^{235}U seeds implanted as temporary brachytherapy sources would be activated by external neutron beam irradiation resulting in capture gammas and secondary fast neutrons in addition to the alpha particles emitted by ^{235}U itself. MCNP was used to evaluate the feasibility of the technique in terms of dose distributions and dose rate. As a follow on to this work, the beta contribution from the ^{235}U fission events was investigated [Li95].

DIAGNOSTIC RADIOLOGY

Computed Tomography

Perhaps one of the most under utilized areas for Monte Carlo calculations in medical dosimetry is in the area of diagnostic radiology. Despite this, Monte Carlo techniques hold significant potential for investigations covering a wide range of diagnostic applications, from

patient exposure and dose to image contrast and resolution. Brockhoff et al were one of the first groups to apply MCNP to the issue of tomographic image reconstruction [Br96]. The simulated a first generation translate/rotate CT scanner. A parallel line source of monoenergetic photons was positioned opposite an array of detector volumes. A MIRD anatomical phantom was placed between the source and detector array. The phantom was rotated and profiles obtained at 2 degree intervals for 180 total degrees. Reconstruction was performed offline. The procedure was repeated using a diagnostic energy spectrum and with a realistic model of a patient obtained from a prior CT scan subsampled to a 64 x 64 matrix to reduce run times. Both simulations resulted in reasonable representations of the original data. Ultimately however, performing over 90 runs to obtain the profiles required to reconstruct a single slice is highly inefficient. Nevertheless, the authors demonstrated that Monte Carlo could be an effective tool for evaluating the physical processes behind tomographic image reconstruction.

Recognizing the inefficiencies in the methods of Brockhoff et al and the need for a complete representation of both the CT scanner and the object to be imaged, Cagnon et al have undertaken a ambitious project for modeling the reconstruction of tomographic images using MCNP using an accurate representation of a CT scanner [Ca99]. Presently, a mono or poly-energetic photon spectrum can be sampled randomly from a fan beam originating from target. For poly-energetic spectra, a cumulative distribution function is constructed from measured or simulated CT bremsstrahlung spectra. The code was modified to provide a phase space model of X-ray source, defining positional location x, y, z and direction vectors u, v, w, and energy (see also: Chetty et al [Ch99a, Ch99b]). The phase space can be varied by the user to provide parameters such as fan width, slice axial thickness, and rotational position about the origin. A set of detector elements configured in an arc is positioned opposite the fan beam. The number of detectors, their size and positions are easily configured by the user to allow optimization of noise or resolution as desired. A model simulating patient tissues: water, muscle, fat and air was defined as series of concentric rings radially symmetric about the origin. The model and reconstructed image are shown in Figure 25. Other factors such as photon energy, photon scatter and beam hardening were also investigated.

The issue of dose received by patients undergoing diagnostic and interventional x-ray procedures. One of the reasons for this is the increasing complexity (and hence time and exposure) of minimally invasive procedures guided by fluoroscopy and angiography. Jansen et al have used Monte Carlo techniques to calculate organ and effective doses from CT procedures [Ja96]. The computed tomography dose index (CTDI) is defined as the integral dose along a line parallel to the z-axis of a CT scanner divided by the slice thickness. CTDI is

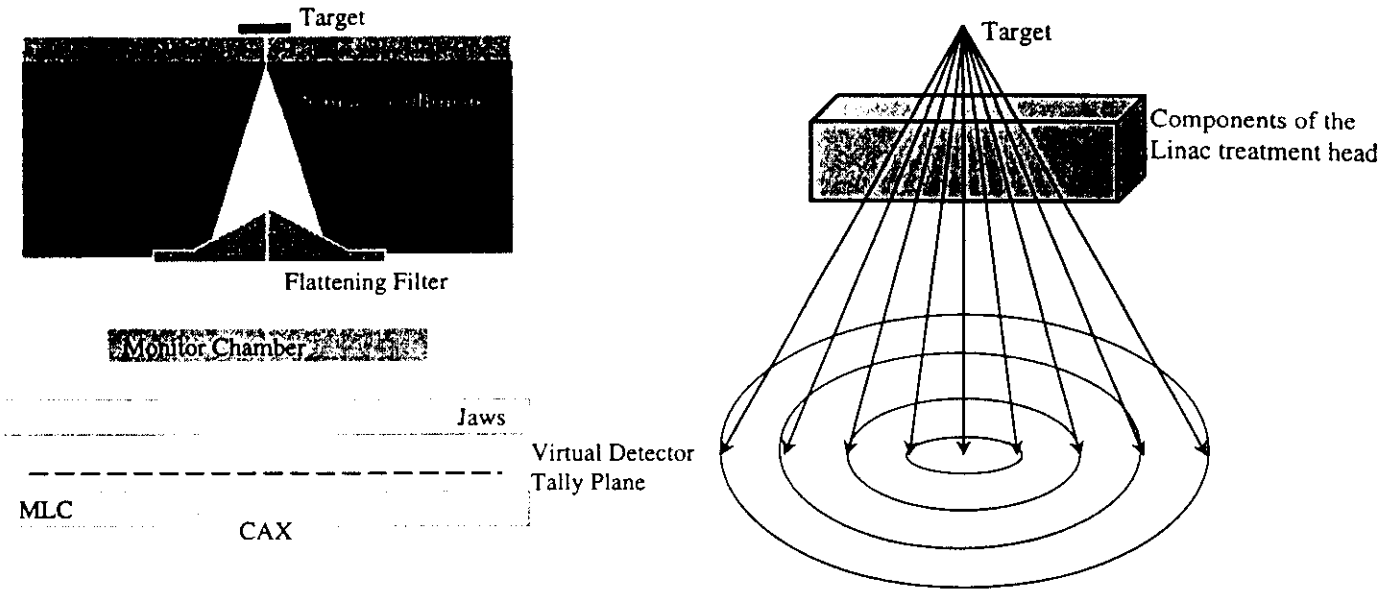

Figure 1. X-ray spectra of high energy medical linear accelerators is performed by transporting electrons on target and following the resulting bremsstrahlung spectra through various components (left). MCNP features "ring detectors," generically referred to as next event estimators (right) for scoring the x-ray spectra.

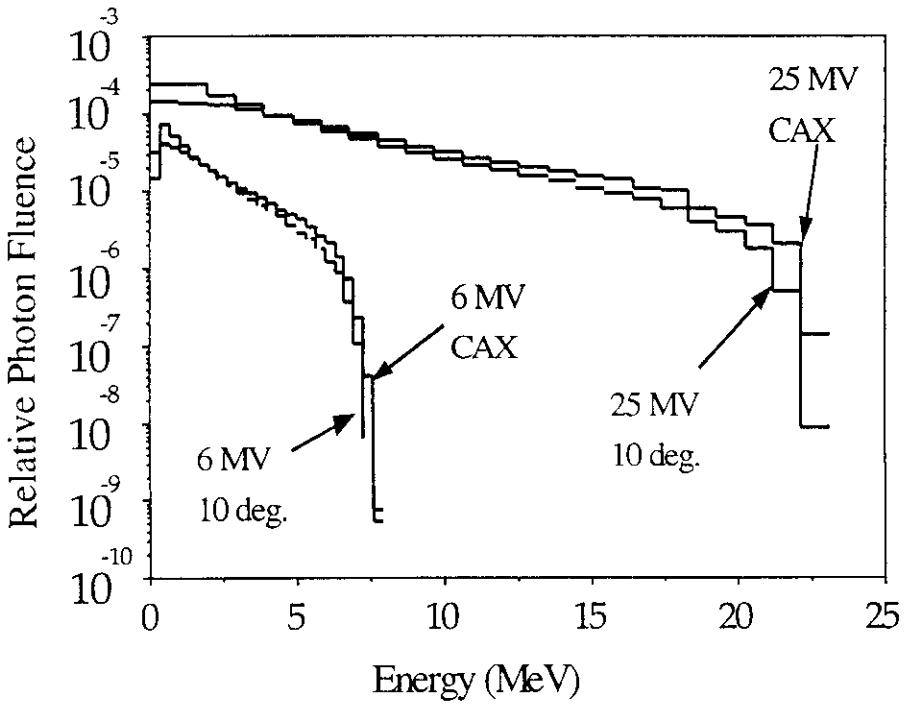

Figure 2. X-ray spectra for nominal 6 and 25 MV beams produced by a Philips SL-25 linear accelerator. From DeMarco et al, 1995.

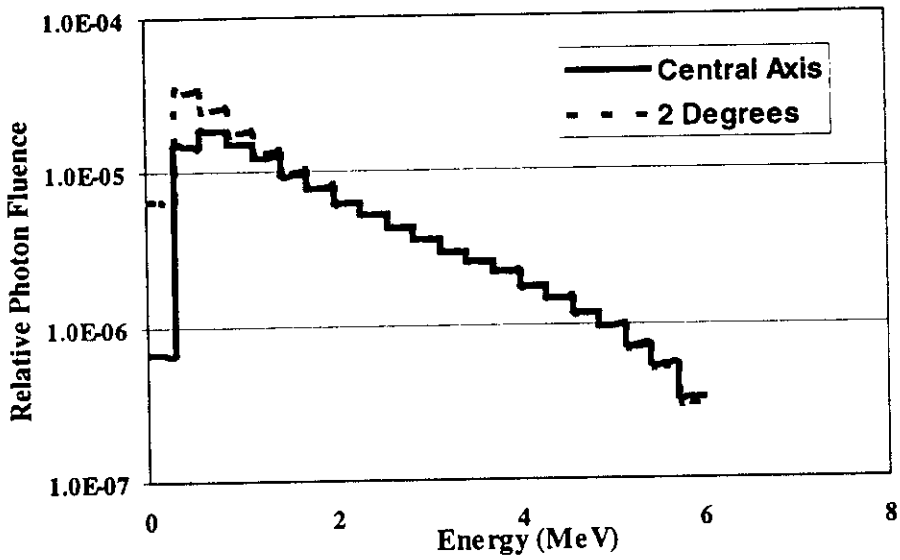

Figure 3. X-ray spectra for nominal 6 MV beams produced Novalis linear accelerator. From Chetty et al, 1999.

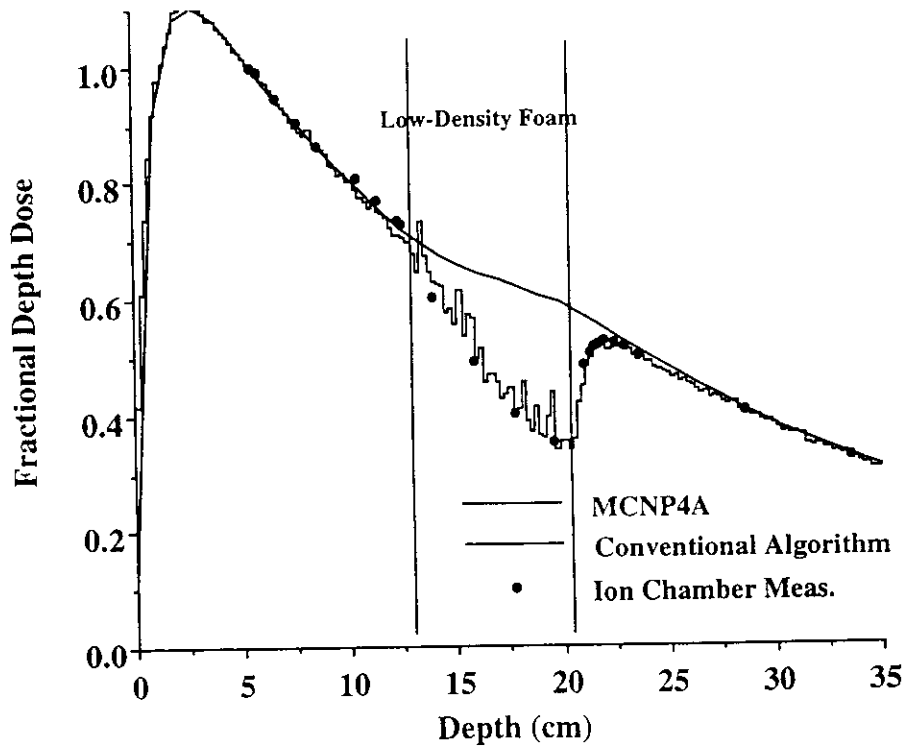

Figure 4. Depth dose benchmark for a 10 MV photon beam traversing a solid water phantom containing a low density region. Measurement and Monte Carlo (MCNP4A) are in excellent agreement while a conventional algorithm (EqTAR) fails to adequately account for the low density region. From DeMarco et al, 1998.

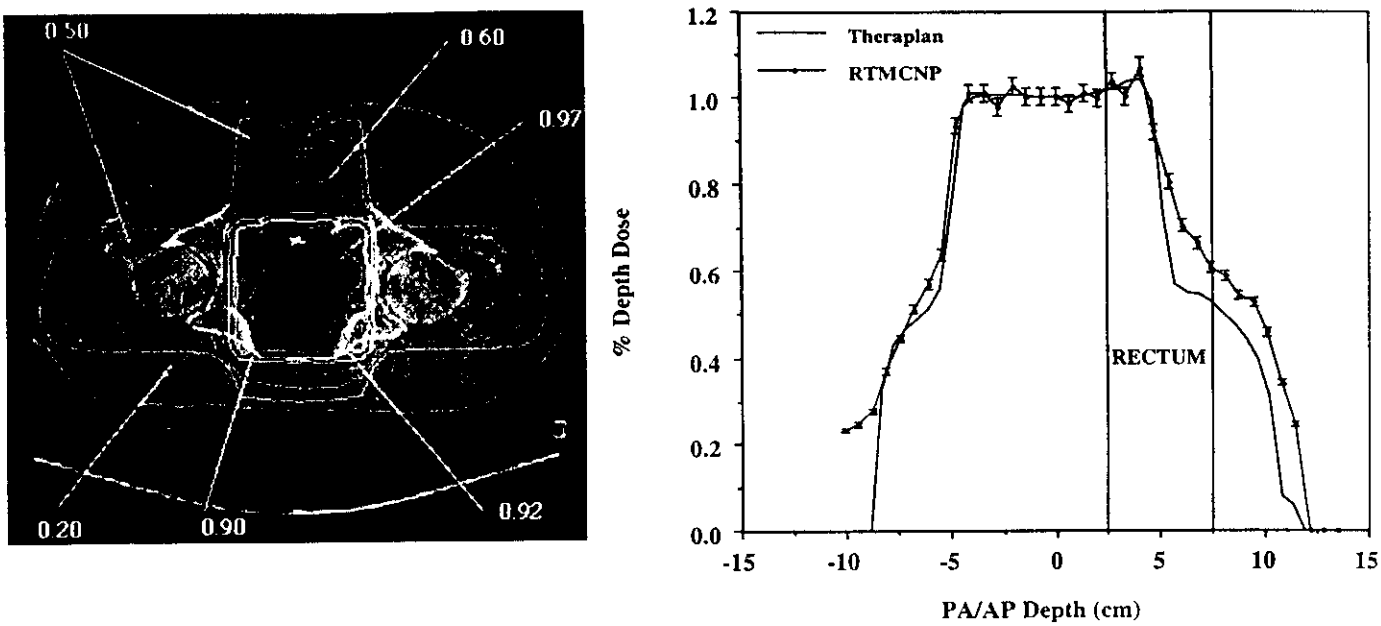

Figure 5. A four-field radiotherapy treatment plans for prostate cancer calculated using MCNP (left). A vertical profile (right) suggests that significant differences can exist between conventional calculations and Monte Carlo, particularly near regions of tissue heterogeneity, in this case a dose limiting structure. From DeMarco et al, 1998.

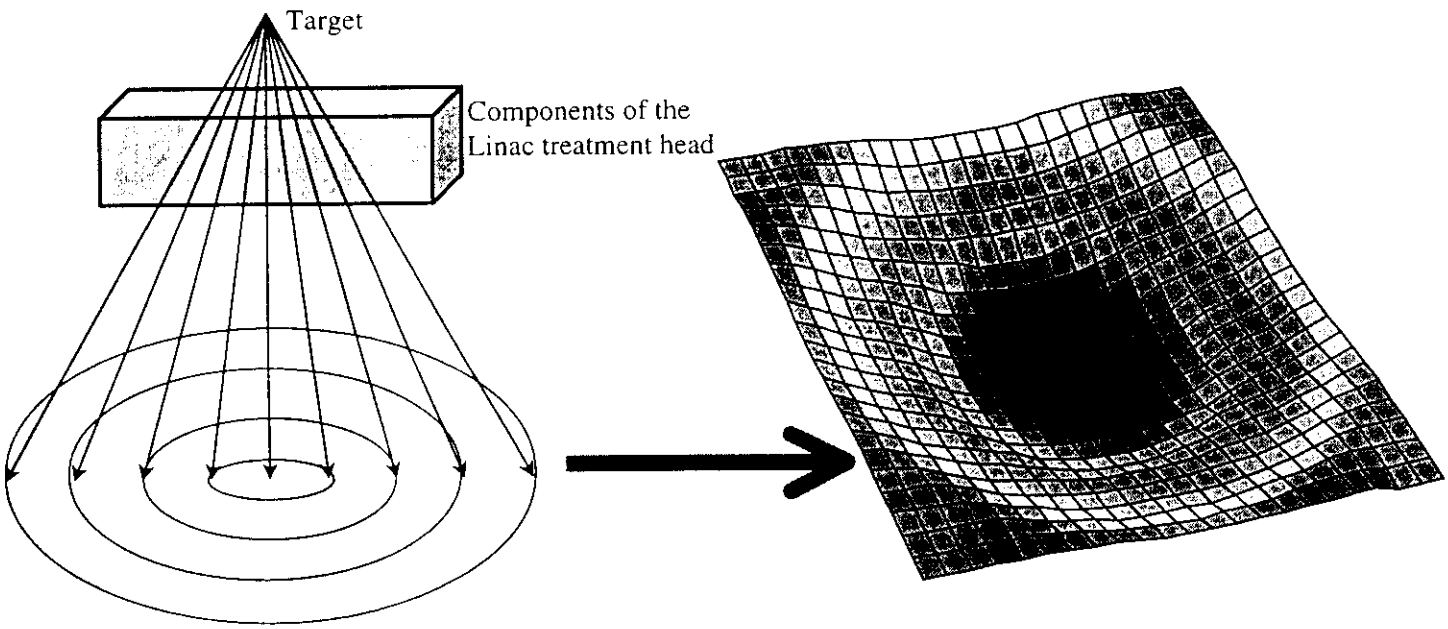

Figure 6. Rotationally symmetric fluence is mapped to a cartesian grid. The photon fluence is lower along the beam CAX relative to the beam edges due to the conical-shaped flattening filter. From Chetty et al, 1999.

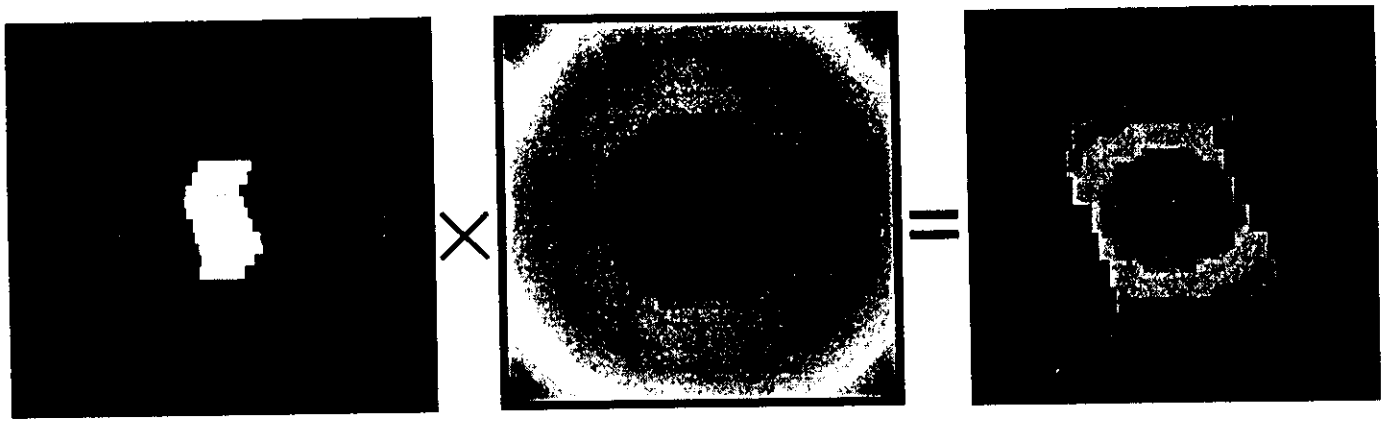

Figure 7. Irregularly shaped beams can be modeled by multiplying the field shape with the fluence map. From Chetty et al, 1999.

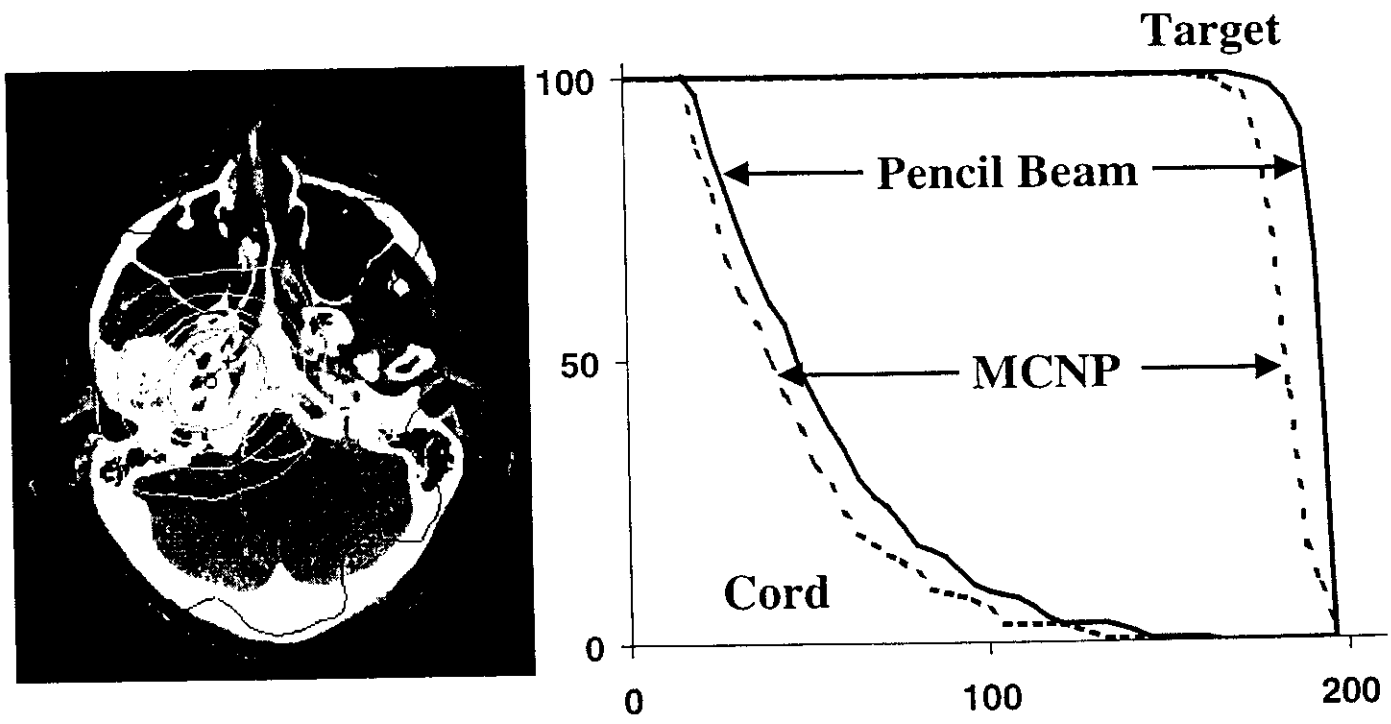

Figure 8. 17 field Monte Carlo treatment plan for a head and neck target (left). As indicated by the dose-volume histogram (right) potentially significant differences exist between the Monte Carlo plan and one calculated using a commercial pencil beam algorithm. From Chetty et al, 1999.

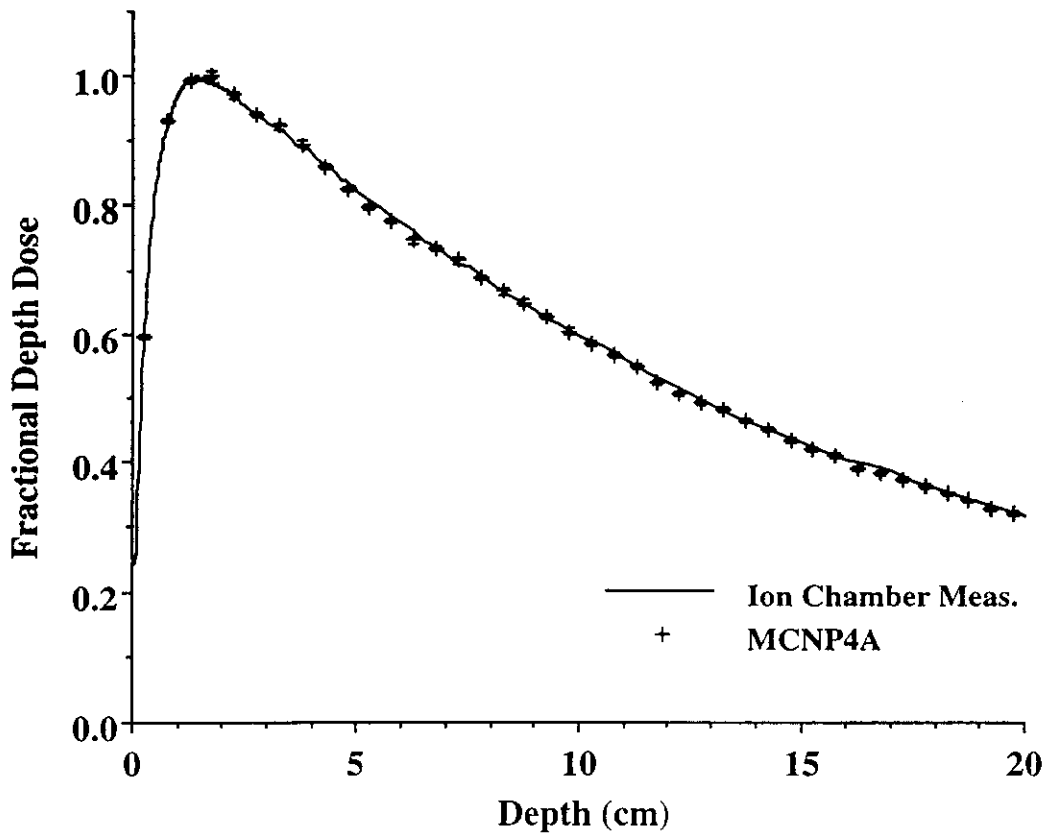

Figure 9. Fractional depth dose in water measured for a 6 MV photon beam collimated to 30 mm in diameter. From Solberg et al, 1998.

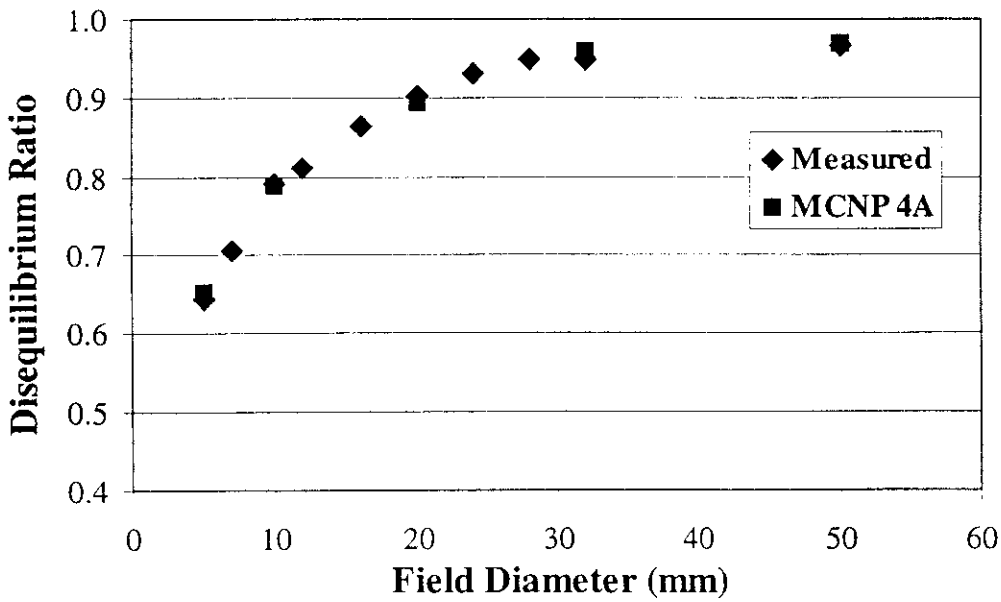

Figure 10. Disequilibrium ratio (defined as the ratio of the dose at the distal edge of a tissue heterogeneity, in this case an air cavity, to the dose at the same point in a homogeneous phantom) as a function of field size for a 10 MV photon beam. From Solberg et al, 1995.

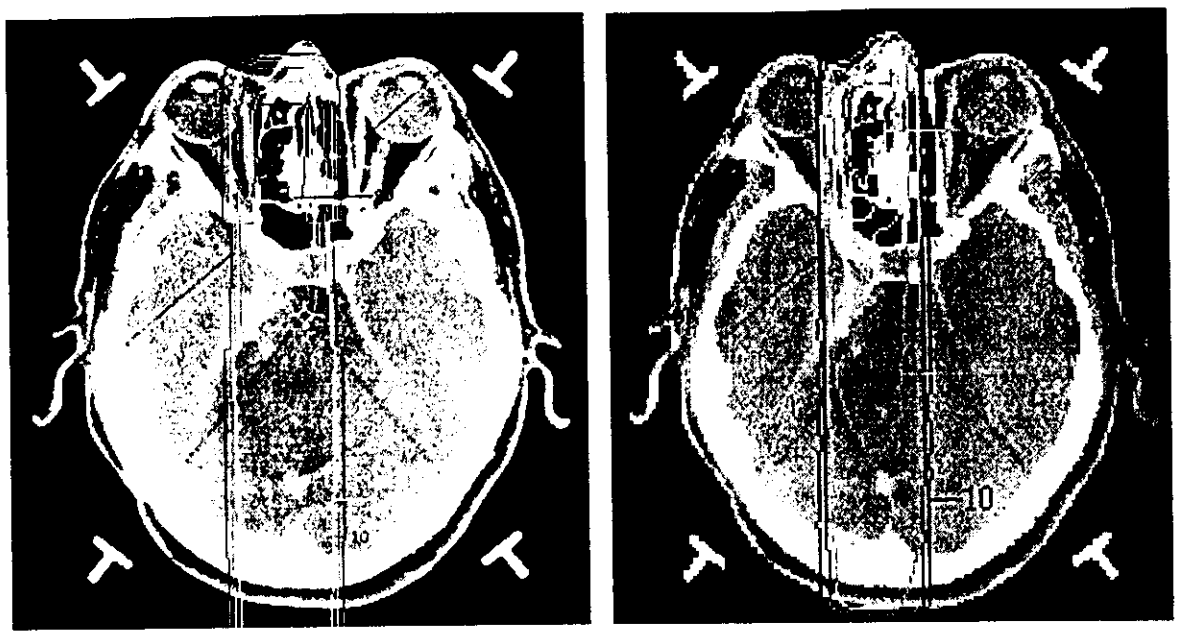

Figure 11. Identical 10 MV treatment plans for a 30 mm diameter AP field calculated using a conventional radiosurgery treatment planning system (left) and MCNP (right). From Solberg et al, 1998.

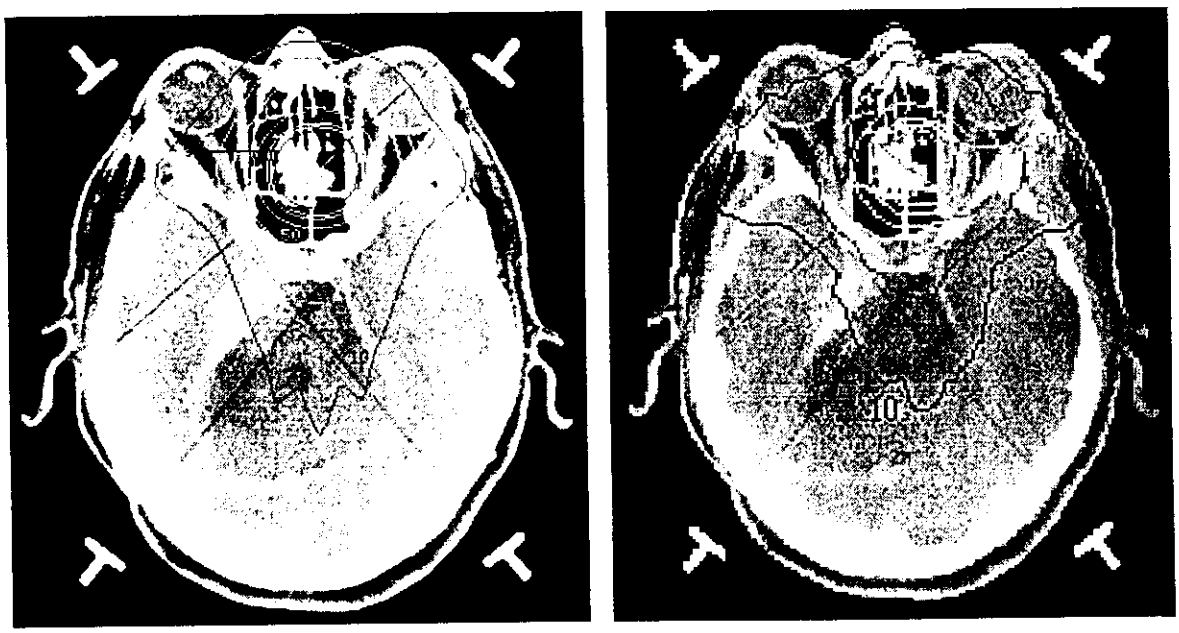

Figure 12. Identical 10 MV treatment plans employing three non-coplanar arcs with a 30 mm diameter collimator calculated using a conventional radiosurgery treatment planning system (left) and MCNP (right). From Solberg et al, 1998.

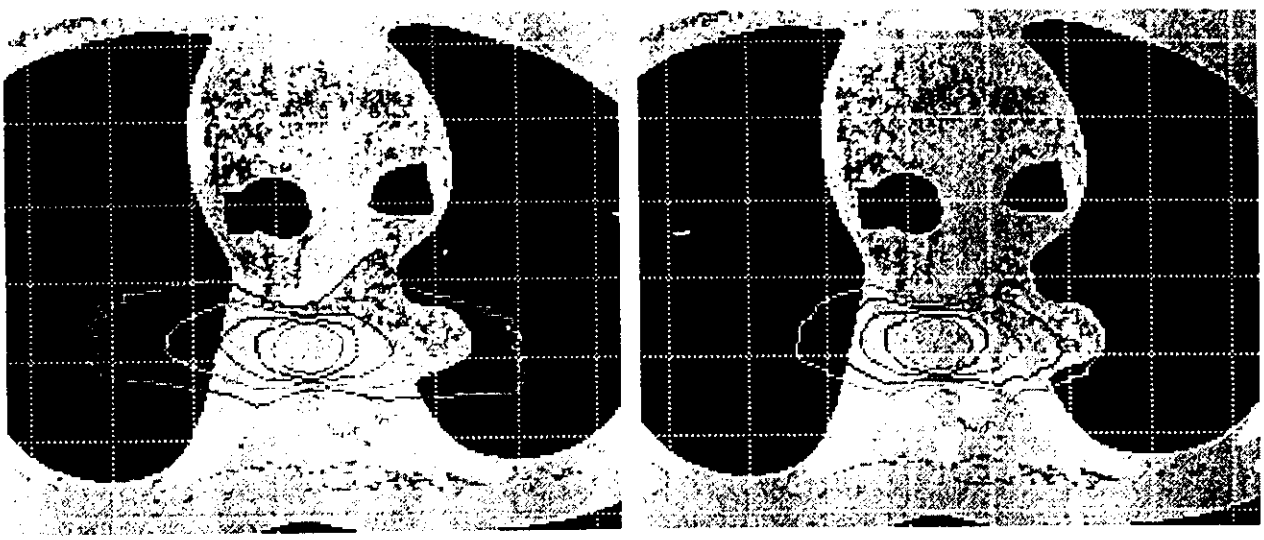

Figure 13. 6 MV treatment plans employing two coplanar arcs of 80 degrees each with a 20 mm diameter collimator. The plan on the left was calculated using a conventional radiosurgery algorithm (TMR/OAR) with the plan on the right was calculated using a MCNP. 82 million primary photon histories to obtain <2% statistics for the Monte Carlo plan. From Medin et al, 1998.

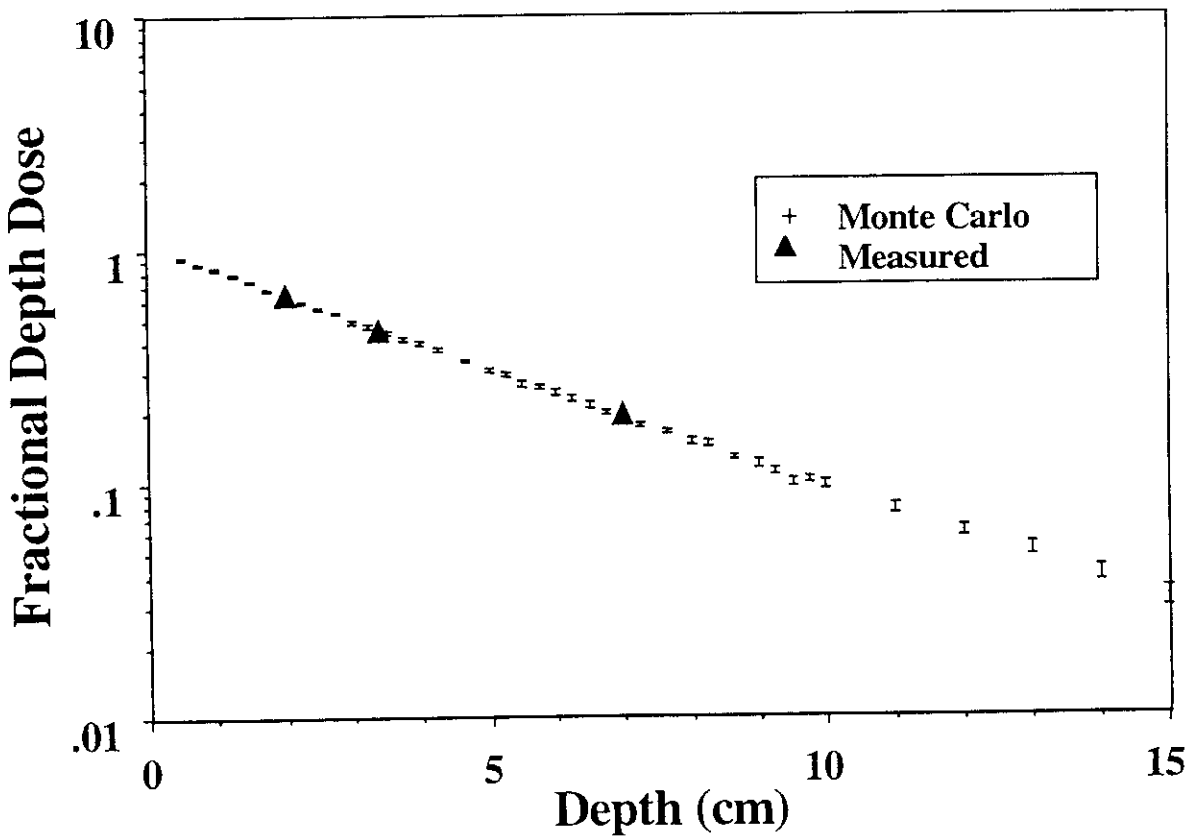

Figure 14. Dose as a function of depth for a 140 kVp x-ray beam. Monte Carlo data were calculated using MCNP while measured data were obtained using an ion chamber in water. Error bars indicate the statistical uncertainty (1σ) in the Monte Carlo calculations. From Solberg et al, 1992.

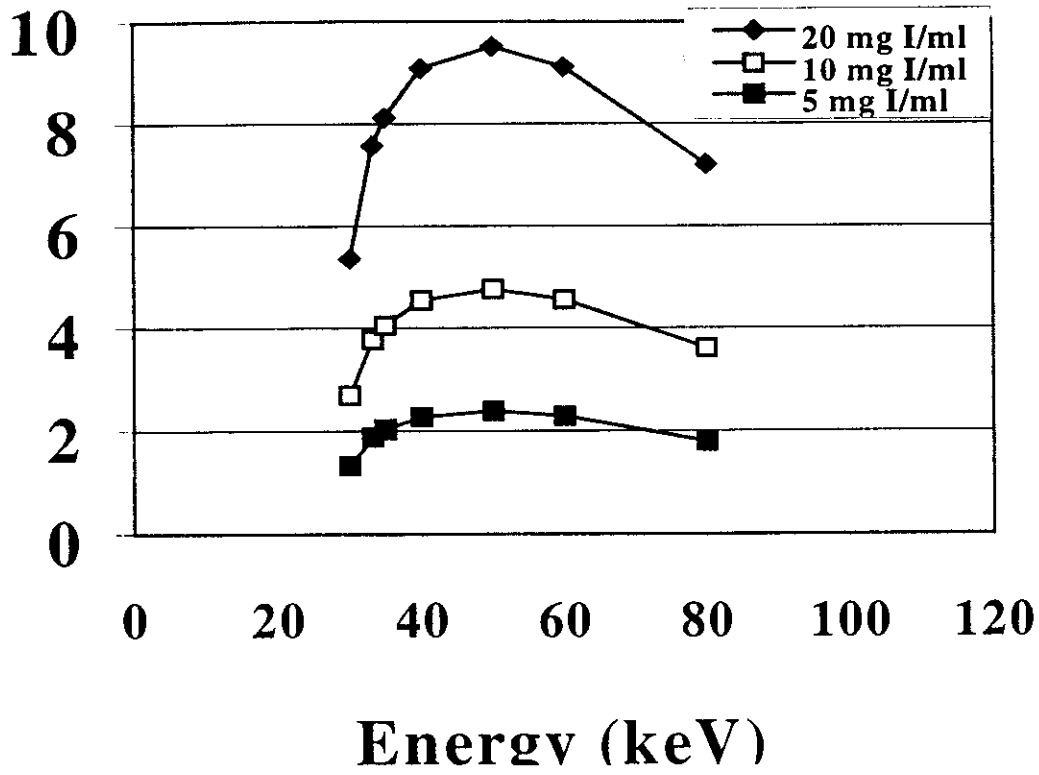

Figure 15. Dose enhancement factor (DEF) as a function of (monoenergetic) x-ray energy for three concentrations of iodine in a tumor. From Mesa et al, 1999.

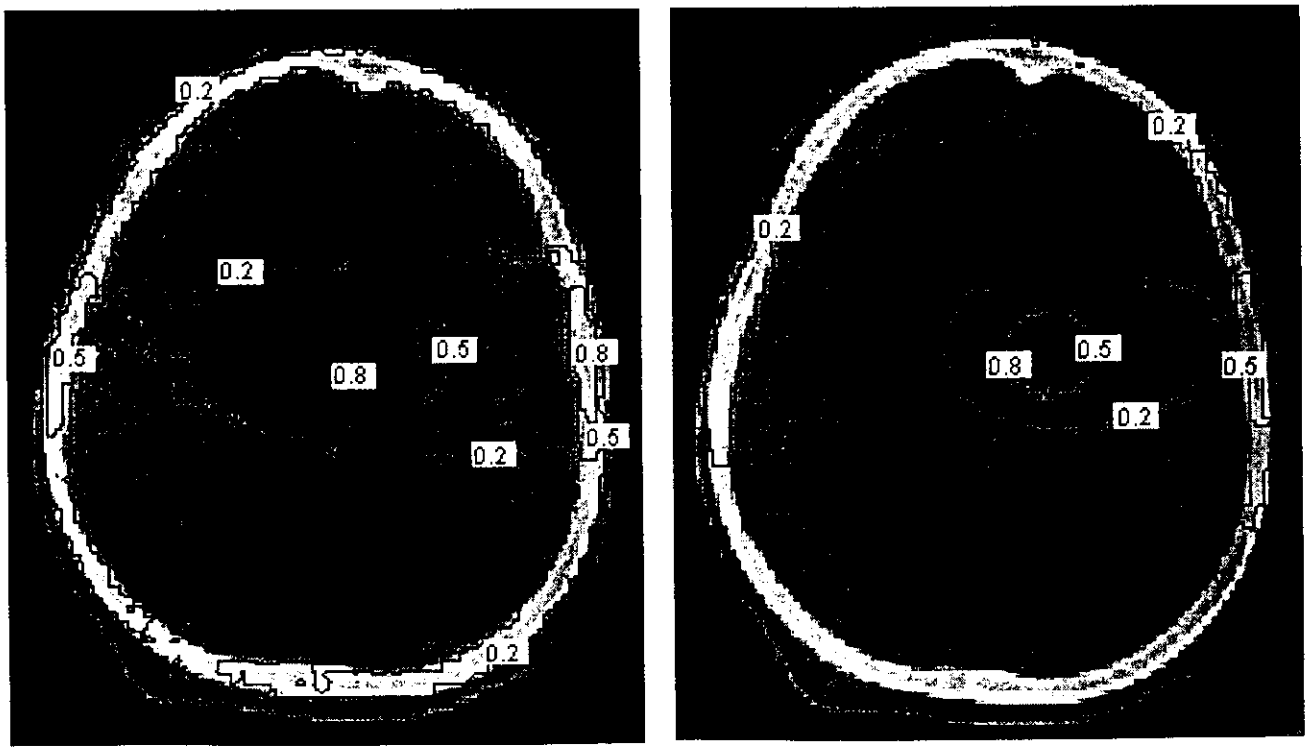

Figure 16. X-ray phototherapy dose distributions for no iodine (left) and 5 mg/ml iodine (right) calculated using MCNP. A 140 kVp spectrum and 3 non-coplanar arcs from a modified CT scanner are included in the simulation. From Mesa et al, 1999.

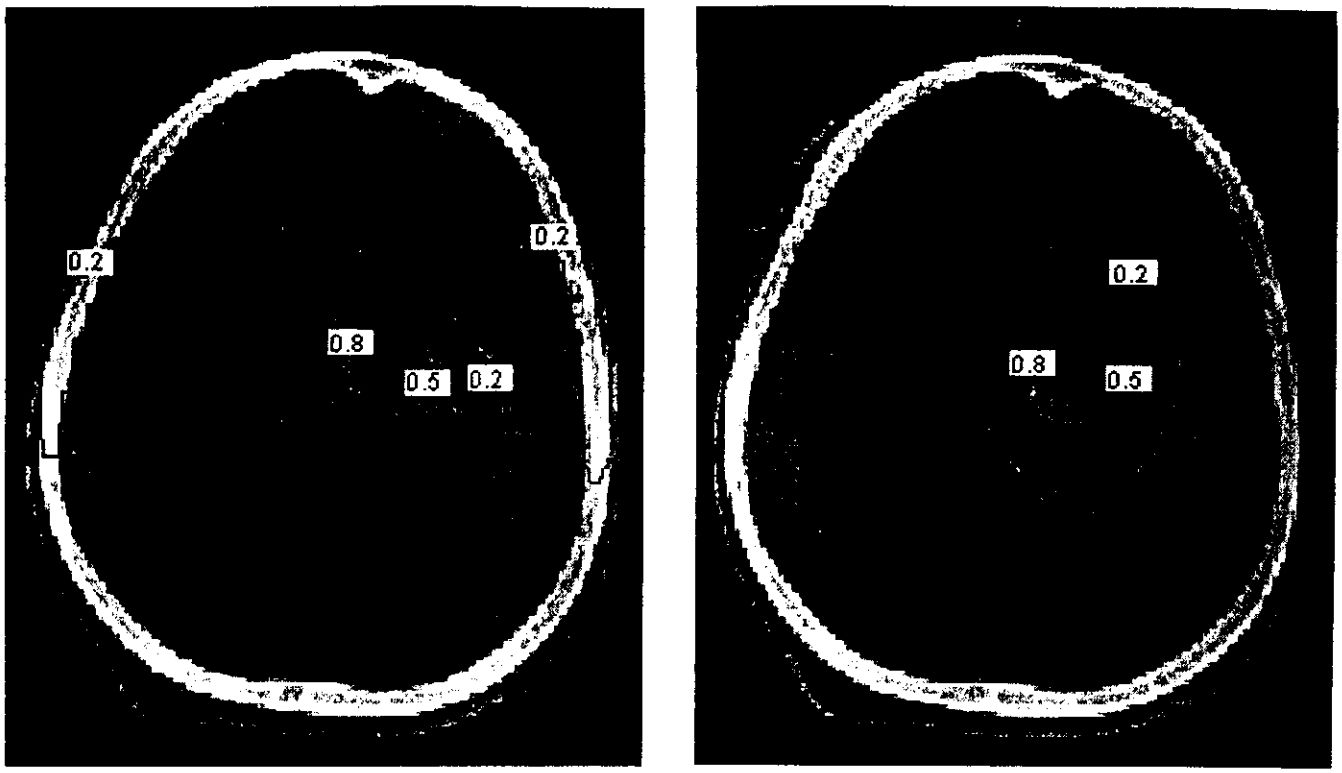

Figure 17. X-ray phototherapy dose distributions for a tumor loaded with 10 mg/ml iodine and irradiated with a 140 kVp beam (left) and a 10 MV beam (right). 3 non-coplanar arcs were used in each MCNP simulation. From Mesa et al, 1999.

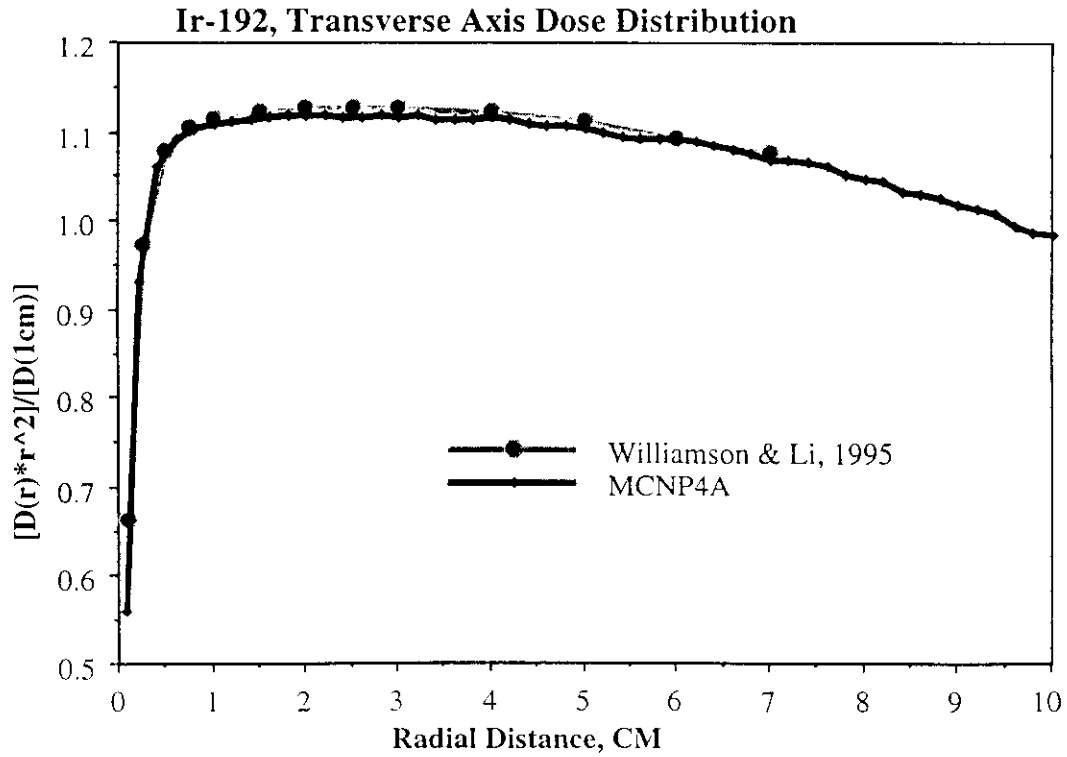

Figure 18. Dose as a function of radial distance (with $1/r^2$ effects removed) for the Microselectron ^{192}Ir source. From Fessenden et al, 1996.

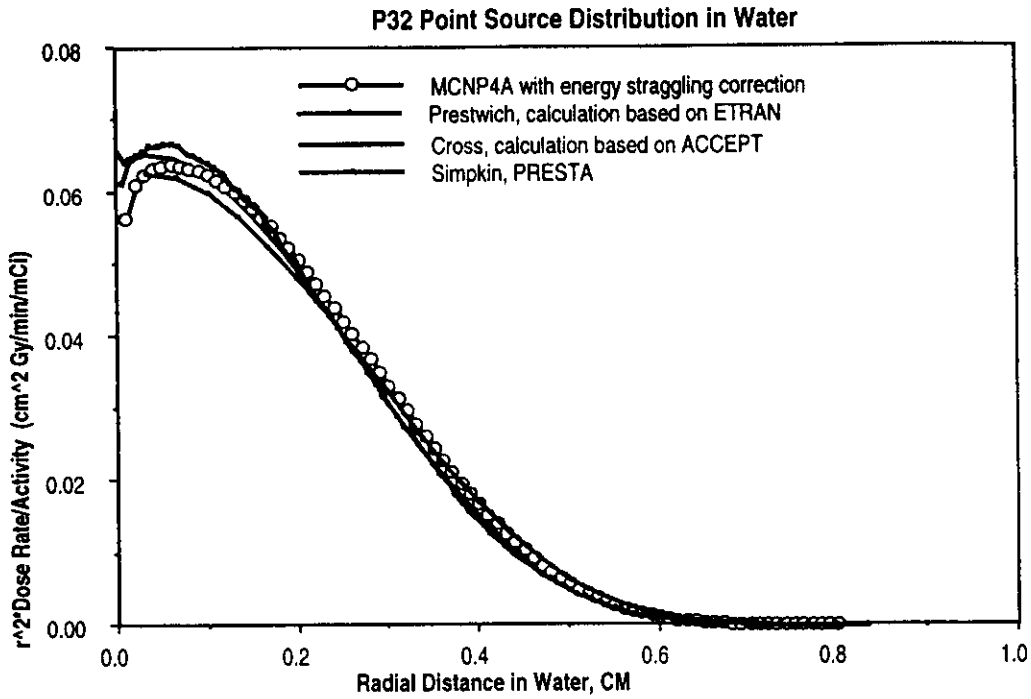

Figure 19. Dose profile with distance in water for a ^{32}P point source. EGS4 calculations from Simpkin et al [Si90]; ETRAN calculations from Prestwich et al [Pr95]; ITS calculations from Cross et al [Cr92]. From Fessenden et al, 1996.

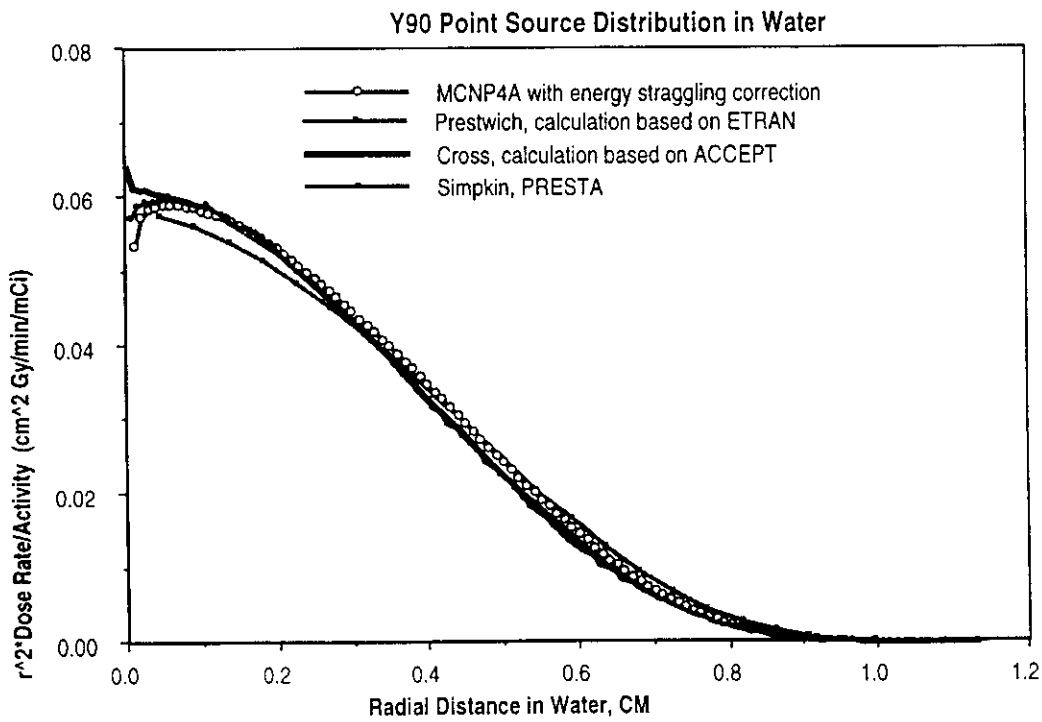

Figure 20. Dose profile with distance in water for a ^{90}Y point source. EGS4 calculations from Simpkin et al [Si90]; ETRAN calculations from Prestwich et al [Pr95]; ITS calculations from Cross et al [Cr92]. From Fessenden et al, 1996.

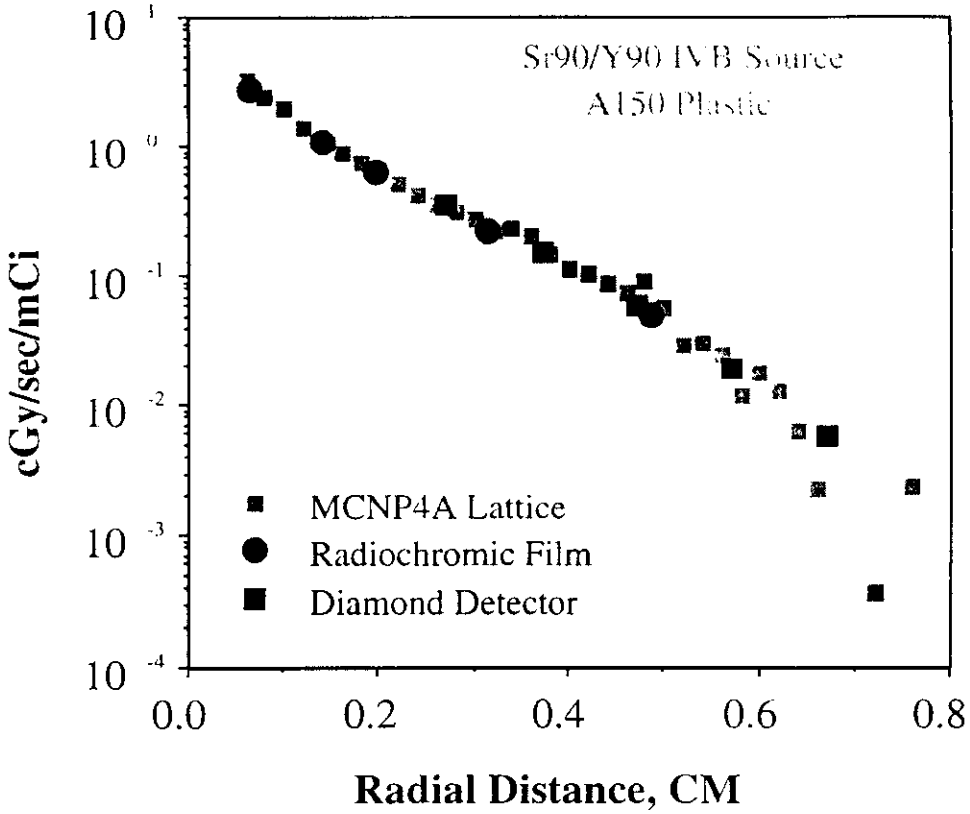

Figure 21. Dose rate per unit activity from a $^{90}Sr/^{90}Y$ intravascular brachytherapy source measured in a solid phantom and calculated using MCNP. From Fessenden et al, 1996.

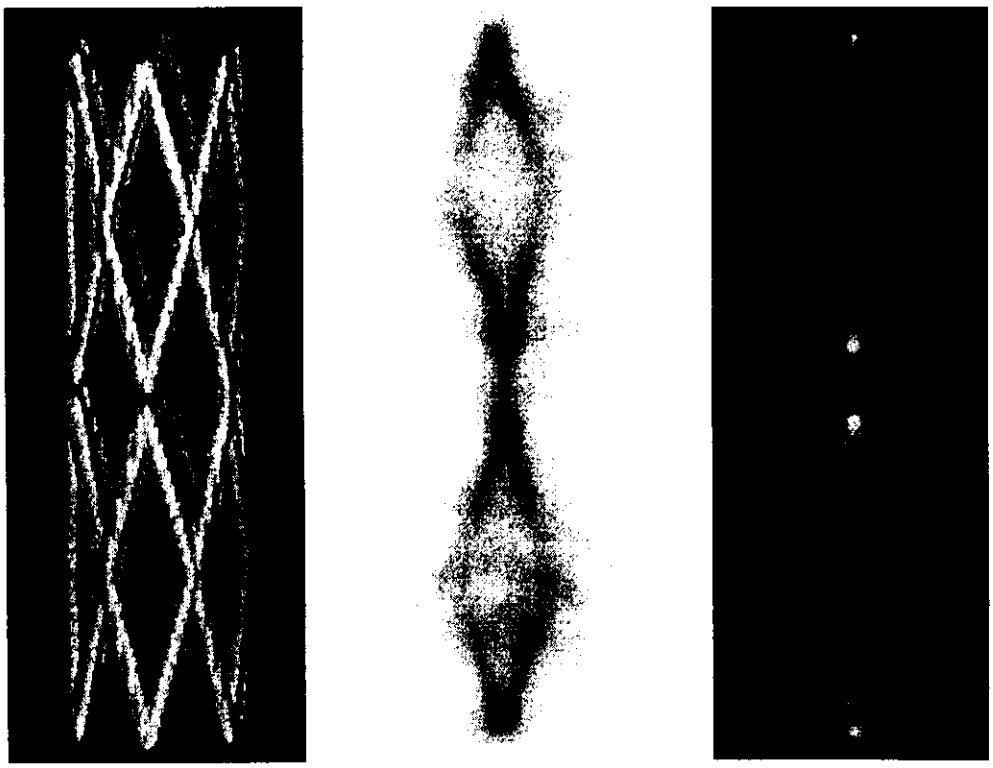

Figure 22. A commercial stent (left) was activated in a proton beam. MCNP calculations were performed for a single strut element and a dose distribution obtained for the entire stent by superimposing the individual elements (right). Calculations were compared to measurement performed using GAF chromic film (middle). From Li et al, 1998.

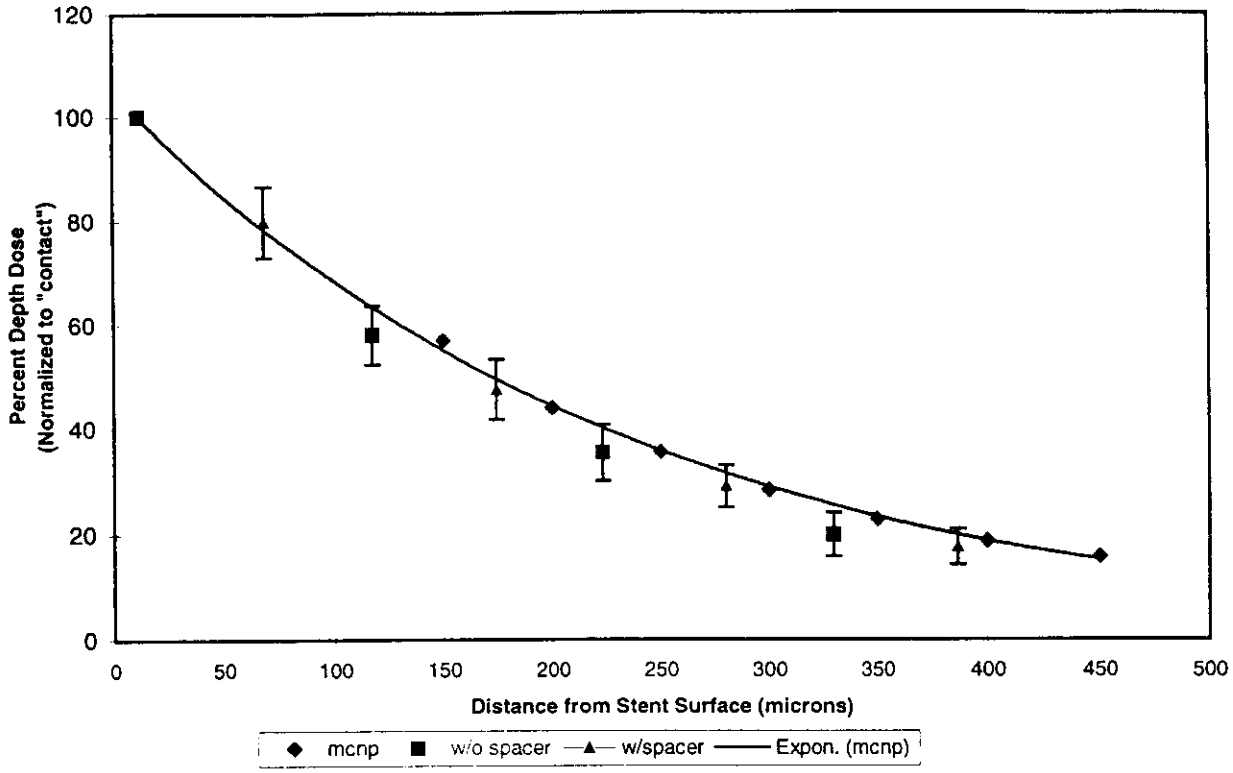

Figure 23. Calculated and measured depth dose of an activated (^{48}V) commercial stent. Data is normalized to "contact." From Li et al, 1998.

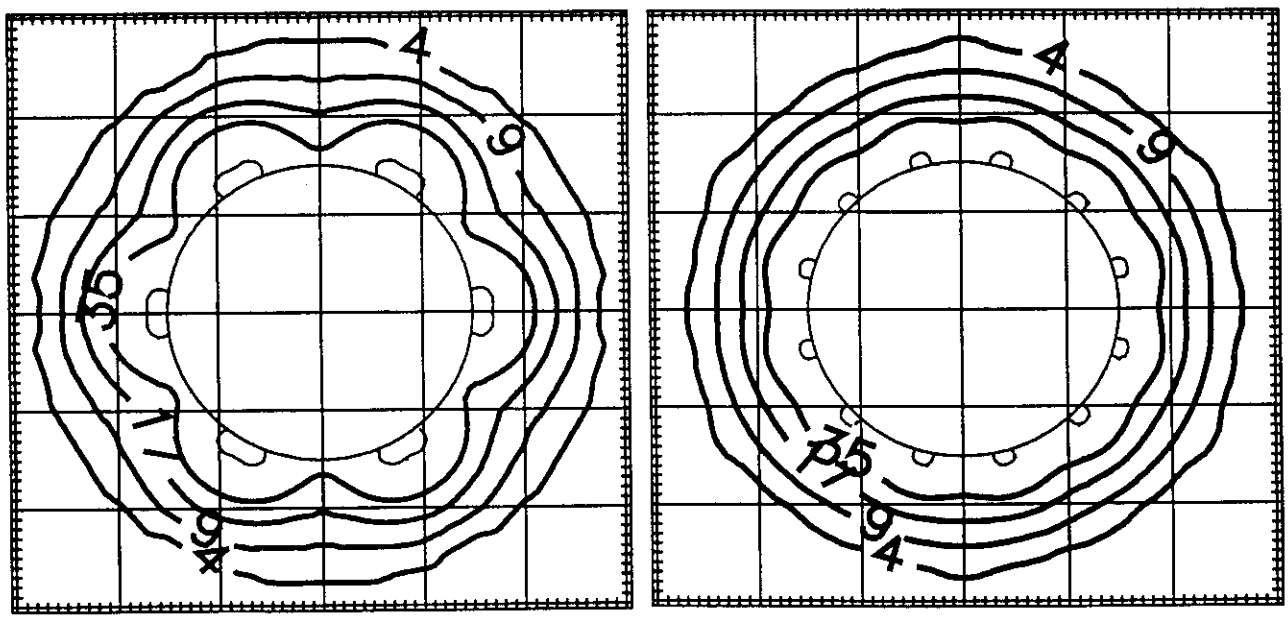

Figure 24. Calculated 2-dimensional cross section dose profiles, in lifetime dose (Gy) per unit activity (μCi), at two different positions for the activated (^{48}V) commercial stent. From Li et al, 1998.

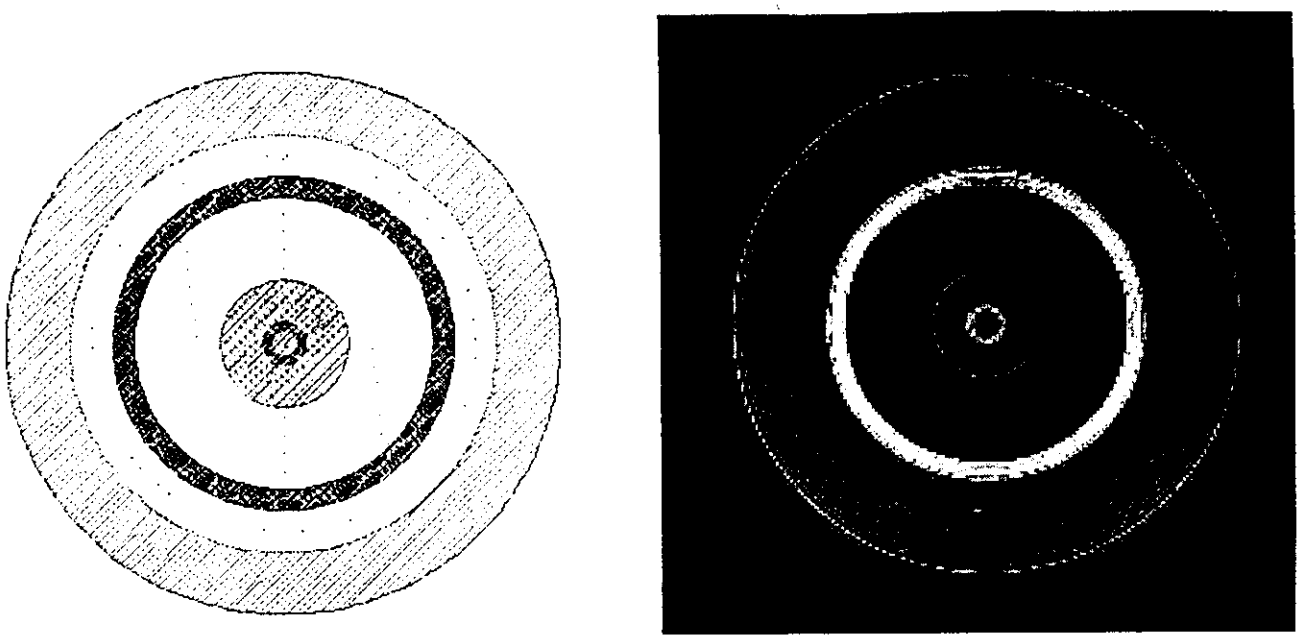

Figure 25. Reconstructed tomographic image (right) from Monte Carlo calculated profiles of the model at left. The materials in order from the outer ring are: water, fat, bone, air, water, bone, water. From Cagnon et al, 1999.

REFERENCES

Agosteo S, Foglio Para A, Maggioni B. Neutron fluxes in radiotherapy rooms. Medical Physics. 20(2): 407-14, 1993.

Andreo P. Monte Carlo techniques in medical radiation physics. Phys. Med. Biol. 36:961-920, 1991.

Arellano AR, DeMarco JJ, Solberg TD. Spectral Characteristics of a Linear Accelerator Dedicated for Radiosurgery. Medical Physics 23(8):1492, 1996.

Berger MJ. "Monte Carlo calculations of the penetration and diffusion of fast charged particles", in Methods in Computational Physics, Vol. 1, B Alder, S Fernbach, and M Rotenberg, eds. Academic Press, New York, 1963.

Berger MJ and Seltzer SM. ETRAN Monte Carlo code system for electron and photon transport through extended media. Radiation Shielding Information Center report CCC-107, 1968.

Bleuel DL, Donahue RJ, Ludewigt BA, Vujic J. Designing accelerator-based epithermal neutron beams for boron neutron capture therapy. Med. Phys. 25(9): 1725-34, 1998.

Bohm TD, Deluca PM Jr, Cox LJ, Maughan RL, Jones DT, Lennox A. Monte Carlo calculations to characterize the source for neutron therapy facilities. Med. Phys. 26(5): 783-92, 1999.

Briesmeister JF. MCNP - A general Monte Carlo N-Particle transport code, version 4A. Los Alamos National Laboratory report LA-12625, 1993.

Briesmeister JF. MCNP - A general Monte Carlo N-Particle transport code, version 4B. Los Alamos National Laboratory report LA-12625-M, 1997.

Brockhoff RC, Estes GP, Hills CR, DeMarco J, and Solberg T. The Application of MCNPTM to Computed Tomography in Medicine, Los Alamos National Laboratory Report, LA-UR-96-135, (1996).

Brugger RM, Herleth WH. Intermediate energy neutron beams from the MURR. Basic Life Sciences. 54: 153-66, 1990.

Burns, GS; Raeside, DE. Monte Carlo estimates of specific absorbed fractions for an I-125 point source in water. Med. Phys. 10(2): 197-8, 1983.

Cagnon C, McNitt-Gray M. DeMarco J. Simulation of CT scanner geometry and physics using Monte Carlo methods. Med. Phys. 26(6): 1063-1064, 1999.

Chen HC and Asau Y. On generating random variates from an empirical distribution. AIIE Trans. 6:163, 1974.

Chetty IC, Solberg TD, DeMarco JJ, Arellano AR, Fogg R. A phase-space model for simulating arbitrary intensity distributions for shaped radiosurgery beams using the Monte Carlo method. Radiosurgery (in press), 1999.

Chetty I, DeMarco JJ, Solberg TD. A virtual source model for Monte Carlo modeling of arbitrary intensity distributions. (in press) Medical Physics, 1999.

Cross WG, Freedman NO, Wong, PY. Beta-ray dose distributions from point sources in an infinite water medium. Health Physics. 63(2): 160-71, 1992.

Dale, RG. A Monte Carlo derivation of parameters for use in the tissue dosimetry of medium and low energy nuclides. Br. J. Radiol. 55(658): 748-57, 1982.

DeMarco JJ, Solberg TD, Wallace RE, Smathers JB. A verification of the Monte Carlo code MCNP for thick target bremsstrahlung calculations. Med. Phys. 22(1):11-16, 1995.

DeMarco JJ, Solberg TD, Smathers JB. A CT-based Monte Carlo Simulation Tool for Dosimetry Planning and Analysis. Med. Phys. 25(1): 1-11, 1998.

DeMarco JJ, Solberg TD, Chetty I, Smathers JB. Efficient sampling algorithms for Monte Carlo based treatment planning. Radiation Physics and Chemistry 53: 229-234, 1998.

DeMarco JJ, Smathers JB, Burnison CM, Ncube QK, Solberg TD. CT-based dosimetry calculations for ^{125}I prostate implants. (in press). Int. J. Radiation Onc. Biol. Physics, 1999.

Evans JF, Blue TE. Shielding design of a treatment room for an accelerator-based epithermal neutron irradiation facility for BNCT. Health Physics. 71(5): 692-9, 1996.

Faddegon BA, Ross CK, Rogers DWO. Angular distribution of bremsstrahlung from 15-MeV electron beams incident on thick targets of Be, Al, and Pb. Med. Phys. 17:727-739, 1991.

Faddegon BA, Ross CK, Rogers DWO. Forward-directed bremsstrahlung of 10-30 MeV electrons incident on thick targets of Al and Pb. Medical Physics, 18:773-785, 1990.

Fessenden KK, DeMarco JJ, Solberg TD, Smathers JB, Wright AE, Kleck JH. Measured and calculated dosimetry for the VariSource HDR source. Med. Phys. 23(6): 1149, 1996.

Fessenden KK, DeMarco JJ, Solberg TD, Rege S, Razavi M, Smathers JB, Almond PR, Xu Z.Monte Carlo dosimetry for beta source selection and design for endovascular irradiation. Int. J. Radiation Onc. Biol. Physics, 36(1-suppl): 401, 1996.

Fitzgerald JJ, Brownell GL, and Mahoney FJ. Mathematical theory of radiation dosimetry. Gordon and Breach Science Publishers, Inc., New York, 1967.

Gupta N, Niemkiewicz J, Blue TE, Gahbauer R, Qu TX. Effect of head phantom size on 10B and 1H[n,gamma]2H dose distributions for a broad field accelerator epithermal neutron source for BNCT. Med. Phys. 20(2): 395-404, 1993.

Halblieb JA and Mehlhorn TA. ITS: the integrated TIGER series of coupled electron/photon Monte Carlo transport codes. Sandia National Laboratory Report SAND 84-0573, 1984.

Hartmann-Siantar CL, Chandler WP, Weaver KA, Albright NW, Verhey LJ, Hornstein SM, Cox LJ, Rathkopf A, Svatos MM. Validation and Perfonnance Assessment of the Peregrine All-Particle Monte Carlo Code for Photon Beam Therapy. Med. Phys. 23:1128, 1996.

Hughes HG. Treating Electron Transport in MCNP. Unpublished Los Alamos National Laboratory report, 1997.

Iwamoto KS, Cochran ST, Winter J, Holburt E, Higashida RT, Norman A. Radiation dose enhancement therapy with iodine in rabbit VSX-2 brain tumors. Radiotherapy and Oncology 8:161-170, 1987.

Iwamoto KS, Norman A, Kagan AR, Wollin M, Olch A, Bellotti J, Ingram M, Skillen R. The CT scanner as a therapy machine. Radiotherapy and Oncology 19:337-343, 1990.

Jansen JT, Geleijns J, Zweers D, Schultz FW, Zoetelief J. Calculation of computed tomography dose index to effective dose conversion factors based on measurement of the dose profile along the fan shaped beam. Br. J. Radiol. 69(817): 33-41, 1996.

Jenkins TM, Nelson WR, and Rindi A (eds). Monte Carlo transport of electrons and photons. Plenum Press, New York, 1988.

Jeraj R, Keall, PJ, Ostwald PM. Comparisons between MCNP, EGS4 and experiment for clinical electron beams. Phys. Med. Biol. 44(3):705-17, 1999.

Kleck JH. Applications of positron emitting tissue activation products in high energy particle and photon therapy. Doctoral Dissertation, University of California, Los Angeles, 1991.

Konijnenberg MW, Mijnheer BJ, Raaijmakers CP, Stecher-Rasmussen F, Watkins PR. An investigation of the possibilities of BNCT treatment planning with the Monte Carlo method. Strahlentherapie und Onkologie. 169(1) :25-8, 1993.

Konijnenberg MW, Dewit LG, Mijnheer BJ, Raaijmakers CP, Watkins PR. Dose homogeneity in boron neutron capture therapy using an epithermal neutron beam. Radiation Research. 142(3) :327-39, 1995.

Kramer GH, Yiu S. Examination of the effect of counting geometry on 125I monitoring using MCNP. Health Physics, 72(3): 465-70, 1997.

Li HB, Brugger RM, Rorer DC, Tichler PR, Hu JP. Design of a high-flux epithermal neutron beam using 235U fission plates at the Brookhaven Medical Research Reactor. Med. Phys. 21(10): 1627-31, 1994.

Li AN, Eigler NL, Litvack F, Whiting JS. Characterization of a positron emitting V48 nitinol stent for intracoronary brachytherapy. Med. Phys. 25(1): 20-8, 1998.

Ling CC, Li WX, Anderson LL. The relative biological effectiveness of I-125 and Pd-103. Int. J. Radiation Onc. Biol. Physics. 32:373-378, 1995.

Liu HB, Brugger RM, Shih JL. Neutron capture therapy with 235U seeds. Med. Phys. 19(3): 705-8, 1992.

Liu HB, Brugger RM, Laster BH, Greenberg DD, Gordon CR, Warkentien LS. Physical and biological doses produced from neutron capture in a 235U foil. Med. Phys. 22(5): 591-5, 1995.

Love PA, Lewis DG, Al-Affan IA, Smith CW. Comparison of EGS4 and MCNP Monte Carlo codes when calculating radiotherapy depth doses. Phys. Med. Biol. 43(5):1351-7, 1998.

Lovelock DMJ, Chui CS, Mohan R. A Monte Carlo model of photon beams used in radiation therapy. Med. Phys. 22: 1387-1394, 1995.

Ma CM, Mok E, Kapur A, Brain S, Findley D, Boyer A. Clinical implementation of a Monte Carlo Treatment Planning System. Med. Phys. 25, A128, 1998.

MacPherson MS, Battista JJ. Dose distributions and dose rate constants for new ytterbium-169 brachytherapy seeds. Med. Phys. 22(1): 89-96, 1995.

Mason D, Battista J, Barnett R, Porter A. Ytterbium-169: Calculated physical properties of a new radiation source for brachytherapy. Med. Phys. 19: 695-703, 1992.

Medin PM ,DeSalles AAF, DeMarco JJ, Selch MT, V Vassilev, Smathers JB, Solberg TD. Radiosurgery for spinal lesions: dosimetric considerations. Med. Phys. 23(6): 1165, 1996.

Medin PM, Solberg TD, DeMarco JJ, Cagnon CH, Chetty IC. A dosimetric comparison of film measurements with three calculation methods for traditional SRS radiation fields in

extracranial target volumes. Proceedings of the 4th International Stereotactic Radiosurgery Society Congress, pg. 55, 1999.

Mello RS, Callison H, Winter J, Kagan AR, Norman A. Radiation dose enhancement in tumors with iodine. Med. Phys. 10, 75-78, 1983.

Mesa AV, Norman A, Solberg TD, DeMarco JJ, Smathers JB. Dose distributions using kilovoltage X-rays and Dose Enhancement from Iodine Contrast Agents. Phys. Med. Biol. (xxx-in press), 1999.

Metzger R, Richardson R, Van Riper KA. A Monte Carlo model for retrospective analysis of shield design in a diagnostic x-ray room. Health Physics, 65(2): 164-71, 1993.

Mo97 Mohan R. "Why Monte Carlo", in Proceedings of the XIIth International Conference on the Use of Computers in Radiation Therapy, DD Leavitt and G Starkschall, Eds. Medical Physics Publishing, 1997.

Nath R, Anderson LL, Luxton G, Weaver KA, Williamson JF, Meigooni AS. Dosimetry of interstitial brachytherapy sources: Recommendations of the AAPM Radition Therapy Committee Task Group No. 43. Med. Phys. 22: 209-234, 1995.

Norman A, Ingram M, Cochran ST, Solberg TD, Ford JM. X-ray phototherapy for Solid Tumors. Academic Radiology 5 (suppl): 177-179, 1998.

Norman A, Ingram M, Skillen RG, Freshwater DB, Iwamoto KA, Solberg TD. X-ray phototherapy for canine brain masses. Radiat. Oncol. Invest. 5: 8-14, 1997.

Pettersson OA, Chiangmai SN, Grusell E, Larsson B. A facility for biomedical experiments with thermal neutrons. Phys. Med. Biol. 38(8): 1081-8, 1993.

Pignol JP, Cuendet P, Brassart N, Fares G, Colomb F, M'Bake Diop C, Sabattier R, Hachem A, Prevot G. Combined use of FLUKA and MCNP-4A for the Monte Carlo simulation of the dosimetry of 10B neutron capture enhancement of fast neutron irradiations. Med. Phys. 25(6): 885-91, 1998.

Pignol JP, Paquis P, Cuendet P, Gibon D, Diop CM, Sabattier R. Beam collimation and bolusing material optimizations for 10boron neutron capture enhancement of fast neutron (BNCEFN): definition of the optimum irradiation technique. Int. J. Radiation Onc. Biol. Physics. 43(5): 1151-9, 1999.

Prestwich WV, Kennett TJ, Kus FW. The dose distribution produced by a 32P-coated stent. Med. Phys. 22: 313-320, 1995.

Rogers DWO and Bielajew AF. Differences in electron depth-dose curves calculated with EGS and ETRAN and improved energy-range relationships. Med. Phys. 13(5): 687-694, 1986.

Rogers DWO, Bielajew AF, Mackie TR, Kubsad SS. The OMEGA Project: Treatment planning for electron-beam radiotherapy using Monte Carlo techniques. Phys. Med. Biol. 35: 285, 1990.

Rogers DWO, Faddegon BA, Ding GX, Ma WM, We J, Mackie TR. BEAM: A Monte Carlo code to simulate radiotherapy treatment units. Med. Phys. 22: 503-524, 1995.

Rose JH, Norman A, Ingram M, Aoki C, Solberg TD, Mesa A. First experience with radiation therapy of human metastatic brain tumors delivered by a computerized tomographic scanner (CTRx). (in press) Int. J. Radiation Onc. Biol. Physics, 1999.

Seltzer SM. "An overview of ETRAN Monte Carlo methods", in Monte Carlo Transport of Electrons and Photons, TM Jenkins, WR Nelson, A Rindi, Eds. Plenum Press, 1988.

Shih JL and Brugger RM. Gadolinium as a neutron capture therapy agent. Med. Phys. 19(3): 733-44, 1992.

Simpkin DJ and Mackie TR. EGS4 Monte Carlo determination of the beta dose kernel in water. Med. Phys. 17: 179-186, 1990.

Solberg TD, Norman A. Iwamoto KS. Radiation Dose Enhancement Therapy for Brain Tumors. Phys. Med. Biol. 37(2): 439-443, 1992.

Solberg TD, Holly FE, DeSalles AAF, Smathers JB. Implications of Tissue Heterogeneity for Radiosurgery in Head and Neck Tumors. Int. J. Radiation Onc. Biol. Physics, 32(1): 235-239, 1995.

Solberg TD, DeMarco JJ, Smathers JB, Holly FE, DeSalles AAF. Monte Carlo Treatment Planning for Stereotactic Radiosurgery. Radiotherapy and Oncology 49:73-84, 1998.

Wallace RE and Fan JJ. Evaluation of new brachytherapy ^{125}I source by AAPM TG-53 formalism. Med. Phys. 25: 2190-2196, 1998.

Wallace SA, Allen BJ, Mathur JN. Monte Carlo calculations of epithermal boron neutron capture therapy with heavy water. Phys. Med. Biol. 40(10): 1599-608, 1995.

Wallace S, Wong T, Fernando W. Monte Carlo dosimetry of the microselectron HDR 192Ir brachytherapy source using MCNP4A. Australasian Physical and Engineering Sciences in Medicine. 21(1): 11-7, 1998.

Wallace S, Allen BJ. CT based 3D Monte Carlo radiation therapy treatment planning. Australasian Physical and Engineering Sciences in Medicine, 21(2):41-50, 1998.

Watanabe Y, Roy JN, Harrington PJ, Anderson LL. Experimental and Monte Carlo dosimetry of the Henschke applicator for high dose-rate 192Ir remote afterloading. Med. Phys. 25(5): 736-45, 1998.

Watanabe Y, Roy JN, Harrington PJ, Anderson LL. Three-dimensional lookup tables for Henschke applicator cervix treatment by HDR 192IR remote afterloading. Int. J. Radiation Onc. Biol. Physics. 41(5):1201-7, 1998.

Wessol DE, Babcock RS, Esty N, Frandsen M, Harkin G, Starkey D, Voss L, Wheeler FJ. "BNCT_RTPE: BNCT radiation treatment planning environment." In: INEEL BNCT Research Program Annual Report 1996, Venhuizen JR Ed. INEEL/EXT-97-00319, 1997.

West JT, SABRINA: An interactive three-dimensional geometry-modeling program for MCNP, Los Alamos National Laboratory report LA-10688-M, 1986.

Wierzbicki JG, Rivard MJ, Waid DS, Arterbery, VE. Calculated dosimetric parameters of the IoGold 125I source model 3631-A. Med. Phys. 25(11): 2197-9, 1998.

Williamson JF; Morin RL; Khan FM. Monte Carlo evaluation of the Sievert integral for brachytherapy dosimetry. Phys. Med. Biol. 28(9): 1021-32, 1983.

Williamson JF. Monte Carlo evaluation of specific dose constants in water for 125I seeds. Med. Phys. 15(5): 686-94, 1988.

Williamson JF; and Quintero FJ. Theoretical evaluation of dose distributions in water about models 6711 and 6702 125I seeds. Med. Phys. 15(6): 891-7, 1988.

Williamson, JF. Comparison of measured and calculated dose rates in water near I-125 and Ir-192 seeds. Med. Phys. 18: 776-786, 1991.

Williamson, JF and Li Z. Monte Carlo aided dosimetry of the Microselectron pulsed and high dose-rate 192Ir sources. Med. Phys. 22(6): 809-819, 1995.

Wong T, Wallace S, Fernando W, Schumer W, Quong G. Dose errors in the near field of an HDR brachytherapy stepping source. Phys. Med. Biol. 44(2): 357-63, 1999.

Woodcock ER, Murphy T, Hemmings PJ, Longworth SC. "Techniques used in the GEM code for Monte Carlo neutronics calculations in reactors and other systems of complex geometries" in Proc. Of the Conf. Applications of Computing Methods to Reactor Problems, Argonne National Laboratory Report ANL-7050, pg .557, 1965.

Wuu CS, Kliauga P, Zaider M, Amols HI. Microdosimetric evaluation of relative biological effectiveness for 103Pd, 125I, 241Am, and 192Ir brachytherapy sources. Int. J. Radiation Onc. Biol. Physics. 36(3): 689-97, 1996.

Yanch JC, Zhou XL, Brownell GL. A Monte Carlo investigation of the dosimetric properties of monoenergetic neutron beams for neutron capture therapy. Radiation Research. 126(1) :1-20, 1991.

Yanch JC, Kim JK, Wilson MJ. Design of a californium-based epithermal neutron beam for neutron capture therapy. Phys. Med. Biol. 38(8):1145-55, 1993.

Zamenhof R, Redmond E, Solares G, Katz D, Riley K, Kiger S, Harling O. Monte Carlo-based treatment planning for boron neutron capture therapy using custom designed models automatically generated from CT data. Int. J. Radiation Onc. Biol. Physics. 35(2): 383-397, 1996.

Zellmer DL, Shadley JD, Gillin MT. Comparisons of measured biological response and predictions from microdosimetric data applicable to brachytherapy. Radiat. Prot. Dosim. 52: 395-403, 1994.